PNAS
www.pnas.org

Main Manuscript for

Extreme hydroxyl amounts generated by thunderstorm-induced corona on grounded metal objects

William H. Brune[1*], Jena M. Jenkins[1], Gabrielle A. Olson[1], Patrick J. McFarland[1], David O. Miller[1], Jingqiu Mao[2], Xinrong Ren[3,4]

[1] Department of Meteorology and Atmospheric Science, Pennsylvania State University, University Park, PA, 16802, USA

[2]Department of Chemistry and Biochemistry and Geophysical Institute, University of Alaska, Fairbanks, Fairbanks, AK, 99775,USA.

[3] Department of Atmospheric and Oceanic Science, University of Maryland, College Park, MD, 20740, USA

[4] Air Resources Laboratory, National Oceanic and Atmospheric Administration, College Park, MD, 20740, USA

* To whom correspondence may be addressed: William H. Brune.

Address: 502 Walker Building, Pennsylvania State University, University Park, PA 16802;

Phone: 814-308-3170; **Email:** whb2@psu.edu

Author Contributions: WHB – supervision, conceptualization, formal analysis, writing original draft and revisions; JMJ – investigation, methodology, formal analysis, writing review and editing; GO – investigation, visualization, writing review and editing; PJM – investigation, formal analysis, visualization, writing review and editing; DOM – methodology, software, writing review and editing; JM – investigation, writing review and editing; XR – investigation, writing review and editing

Competing Interest Statement: The authors declare no competing interests

Classification: Major – Physical Sciences; Earth, Atmospheric, and Planetary Sciences

Keywords: Thunderstorms, atmospheric corona, atmospheric oxidants, hydroxyl, ozone

This PDF file includes:

Main Text
Figures 1 to 5

Abstract

Atmospheric electrical discharges are now known to generate unexpectedly large amounts of the atmosphere's primary oxidant, hydroxyl (OH) in thunderstorm anvils, where electrical discharges are caused by atmospheric charge separation. The question is "Do other electrical discharges also generate large amounts of oxidants?" In this paper, we demonstrate that corona formed on grounded metal objects under thunderstorms produce extreme amounts of hydroxyl (OH), hydroperoxyl (HO_2), and ozone (O_3). Hundreds of parts per trillion to parts per billion of OH and HO_2 were measured during seven thunderstorms that passed over the rooftop site during an air quality study in Houston, TX in summer 2006. A combination of analysis of these field results and laboratory experiments shows that these extreme oxidant amounts were generated by corona on the inlet of the OH-measuring instrument and that corona are easier to generate on lightning rods than on the inlet. In the laboratory, increasing the electric field increased OH, HO_2, and O_3, with 14 times more O_3 generated than OH and HO_2, which were equal. Calculations show that corona on lightning rods can annually generate OH that is 10 to 100 times ambient amounts within centimeters of the lightning rod, and on high-voltage electrical power lines can generate OH that is 500 times ambient a meter away from the corona. Contrary to current thinking, previously unrecognized corona-generated OH, not corona-generated UV radiation, mostly likely initiates premature degradation of high-voltage polymer insulators.

Significance Statement

Corona generated on grounded metal objects by thunderstorms or on high-voltage power transmission lines are known to produce ozone. However, during an air quality study in Houston, TX, thunderstorms produced extreme amounts of hydroxyl (OH), which is the atmosphere's primary oxidant, and hydroperoxyl (HO_2). Laboratory studies confirm that this extreme OH and HO_2 is generated by electrical discharges including corona. Corona generated 28 ozone molecules and one HO_2 molecule for each OH molecule. Calculations show that corona on grounded metal objects under thunderstorms and on high-voltage electrical power transmission lines can generate enough OH near the corona to accelerate the air chemistry and prematurely age materials, including insulators for the high-voltage transmission lines.

Main Text

Introduction

Underappreciated sources of hydroxyl (OH), the atmosphere's primary oxidant, have been recently discovered in thundercloud anvil clouds (1), adding to the existing known OH sources. Atmospheric OH is important because, when chemicals are emitted into Earth's atmosphere, OH reacts to remove many of them. For example, methane, a potent greenhouse gas, is removed from the atmosphere primarily by reaction with OH. However, the subsequent sequence of reactions for many of the chemicals emitted into the atmosphere produce the pollutants ozone (O_3) and small particles, both of which are harmful to human health and important factors in climate change. Thus, any atmospheric phenomena that influences the amount of atmospheric OH also contributes simultaneously to air quality and climate change.

Extreme amounts of OH and another reactive atmospheric constituent hydroperoxyl (HO_2) are generated not just by lightning flashes but also by weaker electrical discharges, even those too weak to be seen or heard. This conclusion came from a combination of airborne observations in thunderstorm anvil clouds during the Deep Convective Clouds and Chemistry (DC3) airborne study in 2012 and subsequent laboratory experiments (1,2). We call HO_x generated by any type of atmospheric electrical discharge LHO_x. Models of electrical discharges have long calculated that lightning flashes and corona discharges produce OH and HO_2 (together called HO_x), but these modeled OH lifetimes were too short for OH to have atmospheric relevance (3-5).

However, contrary to expectations from the models, the OH and HO_2 observed in the anvil clouds and the laboratory live 100 times longer than expected. Presumably, either water vapor is simply dissociated by corona ultraviolet radiation into OH and H, which quickly adds an O_2 to make HO_2, or neutral and ion chemistry accomplishes the same feat (6-8). OH generated in thunderstorm anvils could be responsible for as much as 2 to 16% of total global atmospheric oxidation (1).

Corona discharges, which are stronger than subvisible discharges but weaker than lightning flashes, have been observed for millennia on pointed objects, such as sailing ship masts, when thunderstorms were overhead. It is also known that corona on high-voltage electrodes generate OH under certain conditions (9), but the amount of OH or HO_2 generated was not quantified. If extreme OH and HO_2 can be generated by subvisible discharges in thunderstorm anvils and by corona on high-voltage electrodes, then they should also be generated by coronas that occur when thunderstorms pass over grounded metal objects, such as lightning rods, or on high-voltage electrical power transmission lines (HVTL). Corona-generated OH would react with atmospheric constituents and organic materials near the corona. In this paper, we test this hypothesis using analysis of quantitative observations from the top of an 18-story building, laboratory studies, photochemical box model calculations, and estimates of potential oxidation in the atmosphere and on nearby materials.

Results

Extremely large OH and HO_2 signals were observed with the Ground-based Tropospheric Hydrogen Oxide Sensor (GTHOS) during times when thunderstorms were over the TexAQS II Radical Measurement Project (TRAMP) rooftop site in Houston, Texas (Figs. S1). TRAMP's focus was on Houston air quality (10), so these large signals were noted but not carefully analyzed until recently. Re-examining these signals was motivated by the discovery of extreme OH and HO_2 generated by electrical discharges in thunderstorm anvil clouds and enabled by new analysis methods that produce OH and HO_2 measurements every 0.2 seconds.

During the six-week long study, enhanced HO_x, which is the sum of OH and HO_2, was observed during seven periods when thunderstorms were overhead (Figure 1, Table S1). In these periods, HO_x reached to over 3000 pptv on 23 September, exceeded 1000 pptv on four other occasions, and had a mean value of 120 pptv (Fig. 1A). Enhanced OH reached to over 1000 pptv, with a mean value of 47 pptv. Also plotted in Figures 1C and 1D are HO_2 and OH, both observed and modeled using the RACM chemical mechanism (11). The observed and modeled OH and HO_2 are consistent for times without thunderstorms, thus supporting the GTHOS calibration. Compared to the typical daytime peak values of 10-50 pptv for HO_2 and 0.3-0.6 pptv for OH, these enhanced HO_x values are one to two orders of magnitude higher for HO_2 and two to three orders of magnitude higher for OH. These are the largest concentrations of OH and HO_2 ever observed in the atmosphere, larger even than those observed in thunderstorm anvils clouds.

These extreme HO_x amounts always occurred during thunderstorm activity, which included periods of rain, sometimes heavy (Table S1). All seven periods of enhanced HO_x occurred under overhead thunderstorms (cumulonimbus clouds, Cbs) with low brightness temperatures, which indicates

towering convective clouds. Of these seven periods, three of the largest enhancements occurred primarily in the minutes just before heavy rain began, two occurred primarily during the rain, and two began minutes after the heaviest rain had fallen. For the six times that rain was indicated by OH Rayleigh scattering (called "rain" in Fig. 1) but no enhanced HO_x was observed (Table S1), the satellite visible and water vapor infrared images showed that the rain fell from either edges of small cumulonimbus clouds or from widespread stratocumulus clouds.

Three segments from three days show the detailed behavior of OH and HO_2 (Fig. 2). On 19 August (Fig. 2A), the enhanced HO_x was a series of spikes lasting less than a second each, whereas on 1 and 15 September (Fig. 2B, 2C), it was variable but more continuous. Enhanced HO_x was observed only when the laser wavelength was on the OH absorption line, but the scattering signal in the OH detection axis due to rain occurred also when the laser wavelength was off the OH absorption line. On 15 September during an hourly test period (Fig. 2C), the HO_2 signal dropped to background when the reagent NO was turned off, and the OH spectrum can be seen in both the OH and HO_2 signals during a laser wavelength scan (please see SI for more detail), providing strong evidence that the extreme signals were atmospheric OH and HO_2.

We searched through the GTHOS data sets of a dozen other tower-based field studies. For most of these, no thunderstorms rumbled over the measurement site. Also, for the past 3½ field studies, a Teflon inlet has been placed over the usual metal inlet in order to add a second OH-detection method by scavenging OH with a chemical reactant. This scavenging inlet was added for the second half of the Study of Houston Atmospheric Radical Precursors (SHARP) field study in 2009 (12). In SHARP, the GTHOS inlet was located within two meters of the same location it occupied during TRAMP and, for the first few weeks, had the same grounded aluminum inlet that was used during TRAMP(13) (Figs. S1, 3).

Only one thunderstorm brought heavy rain to the site during those few weeks – on 24 April 2009 between 19:00 and 22:00 CDT (Fig. S2). More than 40 individual sub-second enhanced HO_x spikes were measured. They first occurred a few minutes before the rain began and continued throughout the rainy period. Median values were 1.1 ppbv for OH and for HO_2, and 2.2 ppbv for HO_x. Maximum HO_x was 16 ppbv, more than 4 times larger than the largest peak measured during TRAMP. After the scavenging inlet was placed over the metal inlet, several thunderstorms occurred but no extreme HO_x spikes were observed. These TRAMP and SHARP observations raise the question of the origin of the corona.

Origin of the observed extreme OH and HO_2

The DC3 study demonstrated that electrical discharges in thunderstorm anvils at 9 to 12 km altitude could produce extreme amounts of OH and HO_2 (1), and our previous laboratory studies showed that extreme HO_x amounts could be generated by either visible flashes or subvisible discharges at any tropospheric pressure (2). In that research, visible corona was not studied.

One possible origin is the measurement instrument itself. GTHOS had known interferences for both OH and HO_2 during TRAMP, which have since been remediated. However, laboratory and field experiments all show that the measured extreme OH and HO_2 are inconsistent with these known interferences. Please see the SI for more detail. The extreme OH and HO_2 are 100 times larger than can be produced by known sources. The spikes and variable signals are uncorrelated with the amounts and variation of known interference sources. Also, laboratory experiments demonstrate that measured extreme OH and HO_2 are interference free (2).

The other known mechanisms for generating extreme OH and HO_2 are combustion and high-level energetic radiation, but neither of those sources existed near the GTHOS sampling inlet during TRAMP. Unfortunately, TRAMP had no instruments that could detect electric fields or electrical

discharges. Nevertheless, the coincidence of LHO_x and thunderstorms overhead indicates that these extreme OH and HO_2 values were likely generated by electrical discharges near or on the GTHOS sampling inlet (Table S1). It is likely that either subvisible discharges or corona were the type of electrical discharge and not sparks because sparks cause noise on the GTHOS electronics channels for the microchannel plate detector high voltage (1) and this electronic noise was not observed during TRAMP nor in recent laboratory studies of corona.

These OH and HO_2 mixing ratios of 100 to 2000 pptv translate into concentrations of 2.3×10^9 to 4.6×10^{10} molecules cm^{-3}. At these concentrations, OH and HO_2 rapidly react with many chemical species, but they also react with each other to form H_2O and O_2 with a reaction rate coefficient of $\sim10^{-10}$ cm^3 $molecule^{-1}$ s^{-1}. Thus, the HO_x lifetime from this reaction alone is in the range of 0.22 to 4.3 seconds. For the periods when extreme HO_x was observed, the typical wind speeds measured within 2 m of the GTHOS sampling inlet were 2 to 3 m s^{-1}. As a result, the sources of the extreme HO_x had to have been within 0.5 to 13 m of the GTHOS inlet – somewhere on top of the building.

This estimate of corona origin was further refined by comparing observed ratios of OH to HO_2 to those modeled with a photochemical box model for many LHO_x peaks. Our laboratory studies demonstrate that coronas produce equal amounts of OH and HO_2, and, because OH reacts with many chemical species and decreases more rapidly than HO_2, the OH/HO_2 ratio can be used as a measure of the time since the LHO_x was generated. For seventeen cases selected as being representative, the observed OH/HO_2 was 0.2 to 0.9. In fifteen of the seventeen cases, the observed ratios were achieved in less than 0.2 seconds, with twelve occurring in less than 0.1 seconds (Fig. S3). Note that these reaction times are determined only by the calculated OH/HO_2 ratios with the assumption the OH equals HO_2 initially at time 0. They are not determined by the actual GTHOS measurement times because the GTHOS time resolution is only 0.2 seconds and the exact time that the corona generated OH relative to the start and end of each 0.2 second data bin is unknown. When these times are multiplied by the windspeed, most corona must have originated either from the inlet itself, and, in a few cases, from the extension posts of the scaffolding shown in Fig. S1.

The photochemical box modeling also enabled the calculation of the OH exposure and the OH reaction rates. OH exposure is the integral of OH as a function of time and determines the total amount of each OH reactant that is removed (1, 2). Thus, OH exposure is a more important quantity for discharge-generated OH than the OH concentration is. Generally, a substantial fraction (0.2-0.8, mean: 0.5) of OH is lost to the HO_x-terminating reactions $OH+HO_2\rightarrow H_2O+O_2$, $HO_2+HO_2\rightarrow H_2O_2$, and $OH+NO_2+M\rightarrow HNO_3+M$, where M is N_2, O_2, and H_2O. However, even with this large terminal loss, the mean and median OH exposure was 3×10^9 molecules cm^{-3} s, with a range of 0.3 to 9×10^9 molecules cm^{-3} s. This OH exposure is 1000 times greater than the mean OH exposure generated by normal photochemistry during TRAMP, albeit for a smaller volume and duration.

Laboratory simulations provide OH and HO_2 amounts comparable to TRAMP

To test the hypothesis that corona on the GTHOS inlet could cause the extreme OH and HO_2 values, we performed a series of laboratory experiments described in the Materials and Methods section. Coronas numbered from one to many on the GTHOS inlet depending on the applied electric field (Fig. 3). Positive (negative) coronas occur when the ground metal object is charged positive (negative) relative to the thunderstorm cloud in the atmosphere and the other flat electrode in the laboratory. Note that the structures of positive and negative coronas are quite different, with positive coronas in elongated corona, for which the electrons are accelerated toward the inlet, and negative coronas more like glowing balls, for which the electrons are repelled from the inlet (14,15)

When the laboratory electric field for negative coronas was increased, OH, HO_2, and O_3 increased

proportionally with the laboratory electric field (Fig. 4). NO and NO_2, which are produced in greater amounts in positive corona than in negative corona, were measured to be below ~50-100 pptv, the detection limit of the laboratory instrument. At the highest electric fields in this experiment, HO_x reached more than 20 ppbv and O_3 reached 300 ppbv (Fig. 4). The R^2 for the correlation between HO_x and O_3 is 0.96, indicating that the production of HO_x and O_3 are related. The ratio of O_3 to HO_x is 14 ± 2 for this experiment in which the water vapor fraction was 0.012. This ratio is coincidently the same as that obtained in thunderstorm anvils during the DC3 airborne study in 2012 (16).

Mapping HO_x generated by corona on a GTHOS inlet by sampling the OH, HO_2, and O_3 downwind of the corona enabled a calculation of the OH production rate (Fig. 5). For the experiment described in the Materials and Methods section, the peak HO_x was 4.2 ppbv and the average HO_x production rate was calculated to be $1.8\pm0.9\times10^{15}$ HO_x ($OH+HO_2$) molecules s^{-1}, with OH and HO_2 in equal amounts. This value is a million times the OH production rates generated in a similar volume of Houston air by the well-known urban HO_x sources (11).

If the GTHOS inlet can generate LHO_x, then other grounded metal objects should also be able to generate LHO_x as well. In laboratory experiments, four types of lightning rods were tried: stainless steel static dissipators; pointed copper, rounded copper, and rounded aluminum. The amounts of LHO_x generated on these lightning rods was comparable to that generated on the second GTHOS inlet. However, for both positive and negative coronas, it was easier to initiate coronas on any of the typical types of lightning rods than it was on the GTHOS inlet (Fig. S4). Thus, it is likely that lightning rods and other grounded metal objects on buildings also generate coronas and enhanced OH and HO_2 as thunderstorms pass overhead.

Discussion

These results demonstrate that visible coronas on grounded metal objects generate extreme amounts of OH and HO_2 and that more intense coronas generate more extreme amounts. The amounts of OH and HO_2 generated in the laboratory are also consistent with the amounts observed under thunderstorms during two field campaigns and the amounts generated by subvisible discharges and flashes in thunderstorm anvil clouds.

This observation that coronas can occur on the GTHOS inlet requires that we revisit the possibility that coronas on the Airborne Tropospheric Hydrogen Oxide Sensor (ATHOS) inlet were responsible for at least some of the LHO_x observed in the anvil clouds during DC3 (1). Evidence from the field and laboratory observations ruled out sparks and subvisible discharges, but not weak coronas. However, when the analysis using modeling and the HO_2/OH ratio described earlier and in the SI was applied to the DC3 measurements, 86% of the discharges occurred more than 0.3 seconds (~60 m) in front of the ATHOS inlet, with a median time of 0.56 seconds (~90 m) (Fig. S5). Even the three cases at times less than 0.2 seconds could have occurred in front of the ATHOS inlet because 0.2 seconds is the measurement time resolution. These results provide strong evidence that the enhanced OH and HO_2 observed in anvil clouds during DC3 was not due to coronas on the ATHOS inlet.

The laboratory experiments capture the magnitude of the OH and HO_2 observed during TRAMP and SHARP but do not capture the observed behavior. In some cases, HO_x was generated in ppbv-level sub-second spikes (Fig. 2A), but in other cases it was generated as variable continuum for minutes at a level of a few hundred pptv (Fig. 2B, 2C). We have no solid explanation for the corona generating large sub-second HO_x spikes in some cases and in less amounts but more constant HO_x in others because the characteristics of the electric field and the space charge were not measured during TRAMP. However, it is possible that these differences are due to coronas of different polarity, different electric field strengths, different charge distributions, or a combination of all three.

In the atmosphere, coronas can deplete the charge distributions, reducing the electric fields; charges can move to screen the thunderstorm electric field; or the electric fields can vary, even flipping polarity as the storm passes overhead. In the laboratory, the DC HV supplies continually provide current while maintaining the voltage, thus sustaining the corona. Nonetheless, the comparable amounts of extreme OH and HO_2 observed in TRAMP, SHARP, and the laboratory indicates that the quantities found in the laboratory – HO_x production rates and OH exposures – apply to the TRAMP and SHARP observations as well.

Both lightning rods in a typical urban area and high-voltage electrical power transmission lines are considered as sources of corona-generated OH, In both cases, the corona-generated OH is compared to the OH produced by well-known ambient processes. Please see the SI section 2.1 for more detail.

Consider a lightning rod under the typically 50 thunderstorms that annually pass over Midwestern, Mid-Atlantic, and Southern cities in the United States (17). For the approximately one hour that corona are estimated to be generated on a lightning rod annually, the thunderstorm-induced corona-generated OH is greater than or equal to ambient total OH for ambient air volumes of ~100 m^3 (Fig. S6). Annually, corona-generated OH increases the oxidation by OH as much as a factor of 10 over ambient within ~10 cm of the lightning rod, thus greatly accelerating the degradation of nearby atmospheric constituents and surface materials. For an entire city, the annual impact is confined to the immediate vicinity of the lightning rods (Fig. S7). However, this analysis considers neither downwind effects of corona-oxidized air, the possibility that other pointed metal objects produce corona, or OH generated by lightning. These three effects are difficult to estimate, but all would increase the impact of thunderstorms on atmospheric oxidation in a city.

HVTLs produce corona along the length of the lines and at connections to insulators. Estimates of OH production per meter of line come from a combination of the previously measured O_3 (18,19) and our laboratory results of the relative amounts of OH and O_3 produced. Please see the SI section 2.1. The corona occur continuously, although ~10 times more occurs in foul weather that in fair. Although the estimated amount of corona-generated OH along an HVTL is small compared to total ambient OH generated throughout the planetary boundary layer at the HVTLs, it is more than 50,000 times larger than ambient within 20 cm (volume of 0.1 m^3) of the corona and 500 times larger in a volume of 1 m^3 per meter of line. The distance that enhanced OH is transported downwind of the HVTL can be estimated using a simple Gaussian model (please see the SI for details). This model indicates that trees and structures at the edges of HVTL right of ways are routinely subjected continuously to 10 to 100 times ambient OH. Thus, corona-generated OH could greatly enhance atmospheric oxidation in close proximity to the HVTLs and affect trees more than 10 meters from the HVTLs.

Corona-generated OH initiates the degradation of polymers used for HVTL insulators by breaking a hydrogen-carbon bond (20). Please see the SI section 2.2 for more detail. Corona-generated O_3 is only ~30 times greater than corona-generated OH, based Figure 4, yet it reacts ~100,000 times slower than OH for hydrocarbons with double carbon bonds and not at all for hydrocarbons without double bonds. The comparison between corona-generated UV radiation and OH is more complicated. Based on our laboratory measurements of corona-generated OH and UV radiation with wavelengths less than 290 nm (21), we estimate that the OH flux for a polymer cylinder is 6×10^9 molecules cm^{-2} s^{-1}, 4 times larger than the UV flux of 1.5×10^9 molecules cm^{-2} s^{-1}, with an uncertainty of a factor of ~4 at 68% confidence. If these OH and UV fluxes are equally efficient at breaking this bond, then corona-generated OH is more important than corona-generated UV radiation for the premature degradation of the preferred insulating material, polydimethylsiloxane.

Our discovery of extreme OH generated by corona on pointed grounded surfaces under thunderstorms leads to rethinking the effects of corona on HVTL insulators. Up to now, it has been thought that corona UV radiation in the 200-300 nm wavelength range was responsible for initiating the observed premature degradation of polymer HVTL insulators, which are increasingly replacing old ceramic insulators (22). In the literature, the existence of corona-generated OH appears to be completely unknown. However, according to our estimates, corona-generated OH, not corona-generated UV radiation, initiates most of the premature degradation of polymer insulators used with high-voltage electrical power transmission lines.

Materials and Methods

The TRAMP study and measurements

The TRAMP air quality field study was conducted in Houston, TX in July and August, 2006 (10). The measurements were made from a scaffolding platform on top of the northernmost one of the twin Moody Tower dormitories on the University of Houston main campus (latitude: 29.7176°; longitude: 95.3413°W). The measurements were made at ~70 m above ground level. The campus is 5 km southeast of the tallest buildings in downtown Houston and 6-25 km west-southwest of the primary petrochemical facilities.

The OH and HO_2 measurements were made with the Ground-based Tropospheric Hydrogen Oxides Sensor (GTHOS), which is described in more detail in the SI. In addition to OH and HO_2, the measurement suite included meteorological parameters, photolysis frequencies, O_3, NO, NO_2, CO, peroxides, formaldehyde, and many volatile organic compounds, as shown in Table S2 (10). This measurement suite enabled the modeling of OH and HO_2 both for background conditions and for the rapid decay of OH and HO_2 that occurred following their generation by electrical discharges in the intensified electrical fields under thunderstorms.

Laboratory studies

In the laboratory, OH and HO_2 were measured with GTHOS. The corona was generated on an electrode of interest, which was used as the ground of a pair of electrodes, and the other electrode was a flat aluminum plate (17 cm×16 cm×0.5 cm) to which either negative or positive DC high voltage was applied. The primary electrode of interest was a second GTHOS inlet, the one that was used on TRAMP and SHARP, which was attached to a vacuum pump to simulate the airflow patterns of the actual GTHOS inlet. OH and HO_2 were actually sampled by an inlet attached to GTHOS. We were reluctant to use the actual GTHOS inlet as an electrode for more than a few minutes because of the potential for a spark to damage the GTHOS laser, electronics, or detectors. Four different lightning rods were also studied: stainless steel static dissipators; pointed copper, rounded copper, and rounded aluminum.

Note that this method or generating corona is different from the method used to generate subvisible discharges and sparks previously (2). Those previous discharges were generated by a Tesla coil as short electrical pulses across a pair of tungsten wire electrodes separated by one to two cm.

Corona experiments were run with the electrodes between 2.0 cm to 4.0 cm apart, with applied absolute voltages of ~7 kV to 32 kV with either positive or negative DC high voltage supplies (Information Unlimited HV350REG). A blower blew air past the corona to the GTHOS sampling inlet with a velocity profile that was flat to within 10% over a 10 cm by 6 cm cross sectional area and was set in the range of 1 to 10 m s^{-1} toward the GTHOS inlet, which was located ~20 cm away. Located 1.5 cm to one side of the GTHOS inlet was a ¼" Teflon tube, which was connected to an instruments to measure O_3 (Thermo Scientific 49i) and NO, NO_x, and thus NO_2 (Thermo Scientific

42i and ECO PHYSICS nCLD 855Y). Other measurements include wind speed with a hot-wire anemometer (TSI Inc., 8455-09) and pressure (MKS Instruments Baratron® Type 222), temperature and relative humidity (Vaisala HMT310). Laboratory room air was used for most of these experiments, but, for a few experiments, dry-to-humidified purified air was used. The same results were found no matter the air source.

In some experiments, the laboratory electric field was varied. OH and HO_2, O_3, NO, and NO_2 were simultaneously measured as the voltage applied to the plate was increased from ~7 kV to 32 kV.

In another experiment, corona were generated on the second pumped GTHOS inlet used as the grounded electrode. A voltage of +22.5 kV was applied to the flat plate set 2.0 cm from the second GTHOS inlet. Corona was observed on the sharp edges on the outside of the inlet but never inside the inlet. OH and HO_2 generated by this corona were mapped by moving the corona relative to the sampling inlets. Measurements were taken for 1-2 minutes on positions in a 1.8 cm x 2.0 cm grid. The corona was 22 cm upwind of the GTHOS sampling inlet and the wind speed was 9 m s^{-1}. The total OH production rate (OH molecules s^{-1}) was found by multiplying the OH mixing ratio by the cross-sectional area surrounding each point, adding them together, and then multiplying by the air speed.

Photochemical box modeling

Photochemical box modeling was accomplished with the Framework for 0-D Atmospheric Modeling (F0AM) (23) using the Master Chemical Mechanism v3.3.1 (24,25). Details of the modeling can be found in Brune et al. (1). For this study, the photochemical box model was used for two primary purposes: determining either the OH exposure for the TRAMP LHO_x measurements or the distance between the coronas and the GTHOS sampling inlet.

The OH exposure was determined by multiplying, at each time step, the OH concentration by the width of the time bin, and then summing these products. The distance between the coronas and the GTHOS inlet was determined by a four-step process. First, OH and HO_2 mixing ratios were set equal to each other at half the value of the observed HO_x because our laboratory studies show that OH and HO_2 are generated in equal amounts by coronas. Second, the decays of OH and HO_2 were modeled. Third, the time at which the the modeled OH/HO_2 equaled the observed OH/HO_2 was found. Fourth, this time was multiplied by the measured wind speed to find the distance between the coronas and the GTHOS inlet.

For both purposes, seventeen snapshots of OH and HO_2 were chosen amongst the seven periods that thunderstorms generated enhanced OH and HO_2 during the TRAMP study. These represent the range of initial HO_x mixing ratios measured during TRAMP. The model was constrained to the O_3, NO, NO_2, CO, HCHO, volatile organic compounds, pressure, temperature, and relative humidity measured during the study (Table S2) and run for 100 seconds.

Data and modeling access

The data sets and information on the modeling code used in this study are publicly available: https://doi.org/10.26208/k4ce-zw19. Explanation of the data can be found in a txt file as well as in the SI, Section 3.

Acknowledgments

We thank Barry Lefer and other colleagues at the University of Houston for inviting us to participate in TRAMP and SHARP and all other participants for sharing their data. We thank B. Schrayshuen for helping us with the GIS data for mid-sized cities. This work was supported by the Texas Commission on Environmental Quality grant TERC Project H78 and H86, NSF grant AGS-0209972, and NSF grant AGS-1834711.

References

1. W. H. Brune *et al.*, Extreme oxidant amounts produced by lightning in storm clouds. *Science*, 372, 711-715, DOI: 10.1126/science.abg0492 (2021).

2. J. M. Jenkins, W. H. Brune, D. O. Miller, Electrical Discharges Produce Prodigious Amounts of Hydroxyl and Hydroperoxyl Radicals. *J. Geophys. Res.*, 10.1029/2021JD034557 (2021).

3. R. D. Hill, R. G. Rinker, Production of nitrate ions and other trace species by lightning. J. *Geophys. Res. Oceans,* 86, 3203-3209 (1981).

4. B. A. Bhetanabhotla, B. A. Crowell, A. Coucouvinos, R. D. Hill, R. G. Rinker, Simulation of trace species production by lightning and corona discharge in moist air. *Atmos. Environ.* 19, 1391-1397 (1985).

5. R. A. Boldi, A model of the ion chemistry of electrified convection. MIT PhD thesis, https://dspace.mit.edu/handle/1721.1/51502 (1992).

6. J-S Chang, P. A. Lawless, T. Yamamoto, Corona Discharge Processes, IEEE Trans. Plasma. Sci., 19, 1152-1166 (1991).

7. A. Ershov, A, J. Borysow, J., Dynamics of OH ($X^2\pi$, v=0) in high-energy atmospheric pressure electrical pulsed discharge. *Journal of Physics D: Applied Physics*, *28*(1), 68–74, https://doi.org/10.1088/0022-3727/28/1/012 (1995).

8. A. C. Gentile, M. J. Kushner Reaction chemistry and optimization of plasma remediation of NxOy from gas streams. *Journal of Applied Physics*, *78*(3), 2074–2085. https://doi.org/10.1063/1.360185 (1995).

9. R. Ono, T Oda, Measurement of hydroxyl radicals in pulsed corona discharge, *J. Electronics*, 55, 333-342 (2002).

10. B. Lefer, B. Rappenglück, J. Flynn, C. Haman, Photochemical and meteorological relationships during the Texas-II Radical and Aerosol Measurement Project (TRAMP). *Atmos. Environ.*, 44, 4005-4013, doi:10.1016/j.atmosenv.2010.03.011 (2010).

11. S. Chen, X. Ren, J. Mao, Z. Chen, W. H. Brune, B. Lefer, B. Rappenglueck, J. Flynn, J. Olson, J. H. Crawford, A comparison of chemical mechanisms based on TRAMP-2006 field data. *Atmos. Environ.*, **44**, 4116-4125, 10.1016/j.atmosenv.2009.05.027 (2010).

12. E. Olaguer, C. Kolb, B. Lefer, B. Rappenglück, R. Zhang, J. Pinto, Overview of the SHARP campaign: Motivation, design, and major outcomes. *J. Geophys. Res. Atmos.*, 11,. 2013JD019730. 10.1002/2013JD019730 (2014).

13. X. Ren, D. van Duin, M. Cazorla, S. Chen, J. Mao, L. Zhang, W.H. Brune, J.H. Flynn, N. Grossberg, B. L. Lefer, B. Rappenglück, K.W. Wong, C. Tsai, J. Stutz, J.E. Dibb, B.T. Jobson, W.T. Luke, and P. Kelley, Atmospheric oxidation chemistry and ozone production: Results from SHARP 2009 in Houston, Texas. *J. Geophys. Res.*, 118, 5770–5780, DOI: 10.1002/jgrd.50342 (2013).

14. L. B. Loeb, A. F. Kip, Electrical Discharges in Air at Atmospheric Pressure The Nature of the Positive and Negative Point-to-Plane Coronas and the Mechanism of Spark Propagation. *J. Ap. Phys.*, 10, 142-160, https://doi.org/10.1063/1.1707290 (1939).

15. E. Moreau, P. Audier, N. Benard, Ionic wind produced by positive and negative corona discharges in air, *J. Electrostatics*, 93, 85-96, https://doi.org/10.1016/j.elstat.2018.03.009 (2018).

16. J. Mao, T. Zhao, C. A. Keller, X. Wang, P. J. McFarland, J. M. Jenkins, W. H. Brune, Global impact of lightning-produced oxidants, *Geophys. Res. Let.*, 48, e2021GL095740. https://doi.org/10.1029/2021GL095740 (2021).

17. United Nations Statistics Division, UNdata, data.un.org, accessed March 30, 2022.

18. S. A. Sebo, J. T. Heibel, M. Fryman, C. H. Shih, Examination of ozone emanating from EHV transmission line corona discharges, *IEEE Trans. Pwr. Apparatus and Systems*, PAS-95 (1976).

19. J. F. Roach, F. M. Dietrich, V. L. Chartier, H. J. Nowak, H. J., Ozone concentration measurements on the C-Line at the Apple Grove 750 kV project and theoretical estimates of ozone concentrations near 765 kV lines of normal design. *IEEE Trans. Pwr. Apparatus and Systems*, PAS-97, 693-703 (1978).

20. Kroonblawd, M. P., Goldman, N., Maiti, A., Lewicki, J. P., Polymer degradation through chemical change: A quantum-based test of inferred reactions in irradiated polydimethylsiloxane, *Phys. Chem. Chem. Phys.*, 24, 8142-8157, DOI: 10.1039/d1cp05647f (2022).

21. J. M. Jenkins, G. A. Olson, P. J. McFarland, D. O. Miller, W. H. Brune. Prodigious amounts of hydrogen oxides generated by corona discharges on tree leaves, *J. Geophys. Res. Atmos.*, in revision.

22. B.-H. Youn, C.-S. Huh. Surface degradation of HTV silicone rubber and EPDM used for outdoor insulators under accelerated ultraviolet weathering condition, *IEEE Trans. Dielectrics Electrical Insulation*, 12, 1015-1024. (2005).

23. G. M. Wolfe, M. R. Marvin, S. J. Roberts, K. R. Travis, J. Liao, The framework for 0-D atmospheric modeling (F0AM) v3.1. *Geosci. Model Dev.*, 9, 3309-3319 (2016).

24. S. M. Saunders, M. E. Jenkin, R. G. Derwent, M. J. Pilling, Protocol for the development of the Master Chemical Mechanism, MCM, v3 (Part A): tropospheric degradation of non-aromatic volatile organic compounds. *Atmos. Chem. Phys.* 3, 161-180 (2003).

25. M. E. Jenkin, S. M. Saunders, V. Wagner, M. J. Pilling, Protocol for the development of the Master Chemical Mechanism, MCM, v3 (Part B): tropospheric degradation of aromatic volatile organic compounds. *Atmos. Chem. Phys.* 3, 181-193 (2003).

Figures legends

Figure 1. TRAMP OH and HO_2 measurements versus Central Standard Time (CST). Shown are (A) rain-induced GTHOS scattering signal (arbitrary units), designated as "rain"; (B) periods with extreme HO_x (gold) and OH (blue) mixing ratios (pptv), indicating LHO_x; (C) ambient HO_2 from measurement (gold) and model (black); and (D) ambient OH from measurement (blue) and model (cyan).

Figure 2. Three examples of OH and HO_2 generated by electrical discharges versus time (CST). Three minutes were chosen for August 19 (A), Sept 1 (B), and Sept 15 (C). In A and B, dashed lines indicate times the laser wavelength is on an OH absorption line. In C, the dot-dashed line indicates an hourly instrument test period including a wavelength scan of the laser (15:31-15:33, with the OH $Q_1(2)$ fluorescence near 15:32) and the thicker dashed line indicates a time when the reagent NO was turned off, so that only OH was measured.

Figure 3. Coronas generated on the edges of the GTHOS inlet in the laboratory. In A are three positive elongated coronas and three faint wisps, with the inlet grounded and the overhead plate negatively charged. In B are negative ball-shaped coronas, with the inlet grounded and the overhead plate positively charged. For these pictures, the DC voltage was 25 kV and the inlet to plate separation was 2.5 cm. The flat part of the inlet is 19 mm in diameter.

Figure 4. HO_x and O_3 on a GTHOS inlet as a function of the laboratory electric field. A negative corona with an electrode separation of 2 cm was used in this experiment, but positive coronas give similar behavior, although different values as a function of electric field.

Figure 5. Laboratory map of HO_x mixing ratio for a corona on a second pumped GTHOS inlet used as the positive electrode. Peak HO_x was 4.2 ppbv, with OH and HO_2 abundances equal to within 10%. The calculated HO_x production rate is 1.8×10^{15} molecules s^{-1} (please see SI for details).

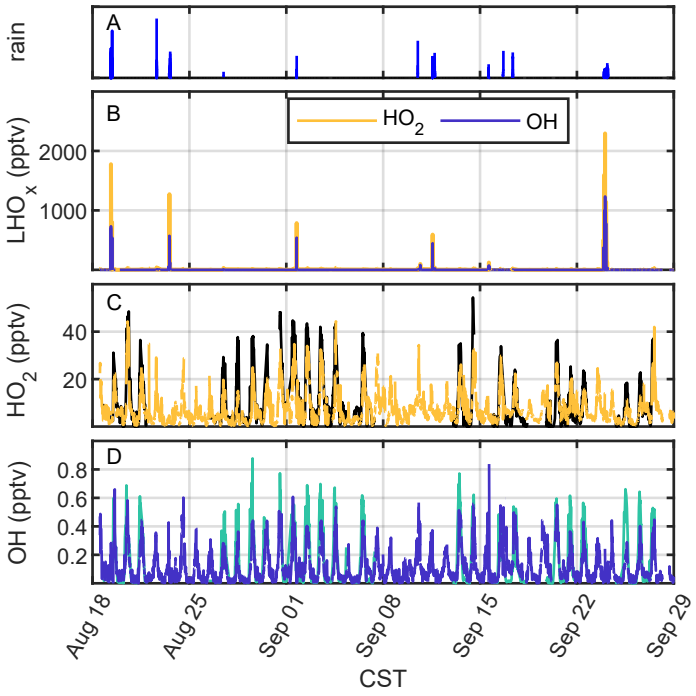
A
rain
B
HO2
OH
LHOx (pptv)
2000
1000
C
HO2 (pptv)
40
20
D
OH (pptv)
0.8
0.6
0.4
0.2
Aug 18
Aug 25
Sep 01
Sep 08
Sep 15
Sep 22
Sep 29
CST

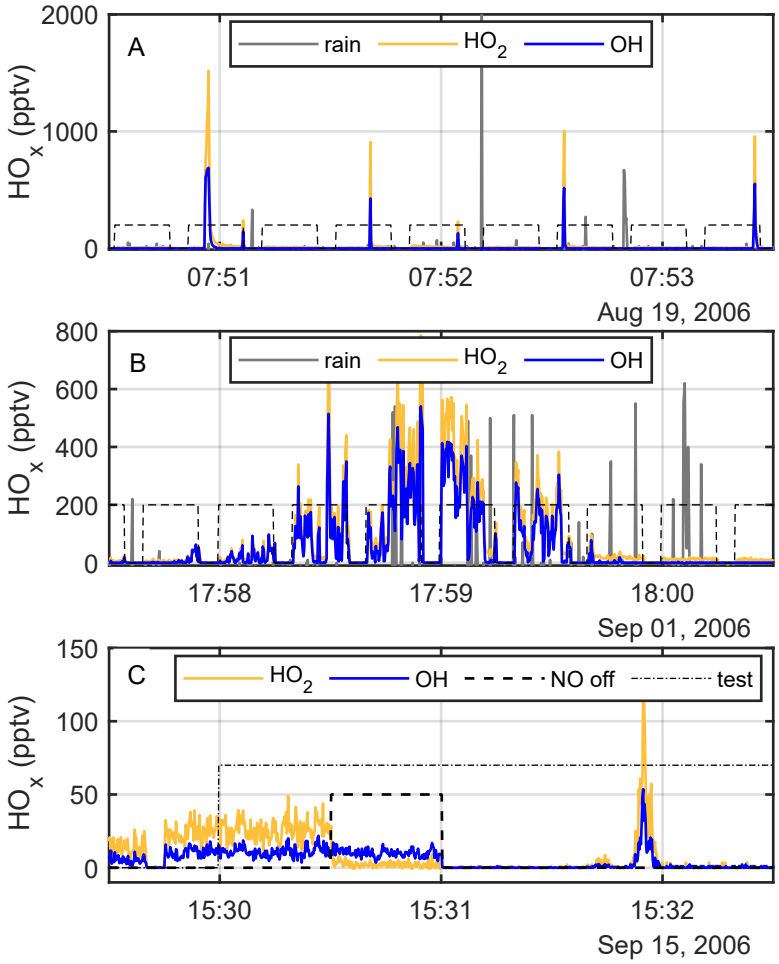
A
rain
HO2
OH
HOx (pptv)
2000
1000
0
07:51
07:52
07:53
Aug 19, 2006
B
rain
HO2
OH
HOx (pptv)
800
600
400
200
0
17:58
17:59
18:00
Sep 01, 2006
C
HO2
OH
NO off
test
HOx (pptv)
150
100
50
0
15:30
15:31
15:32
Sep 15, 2006

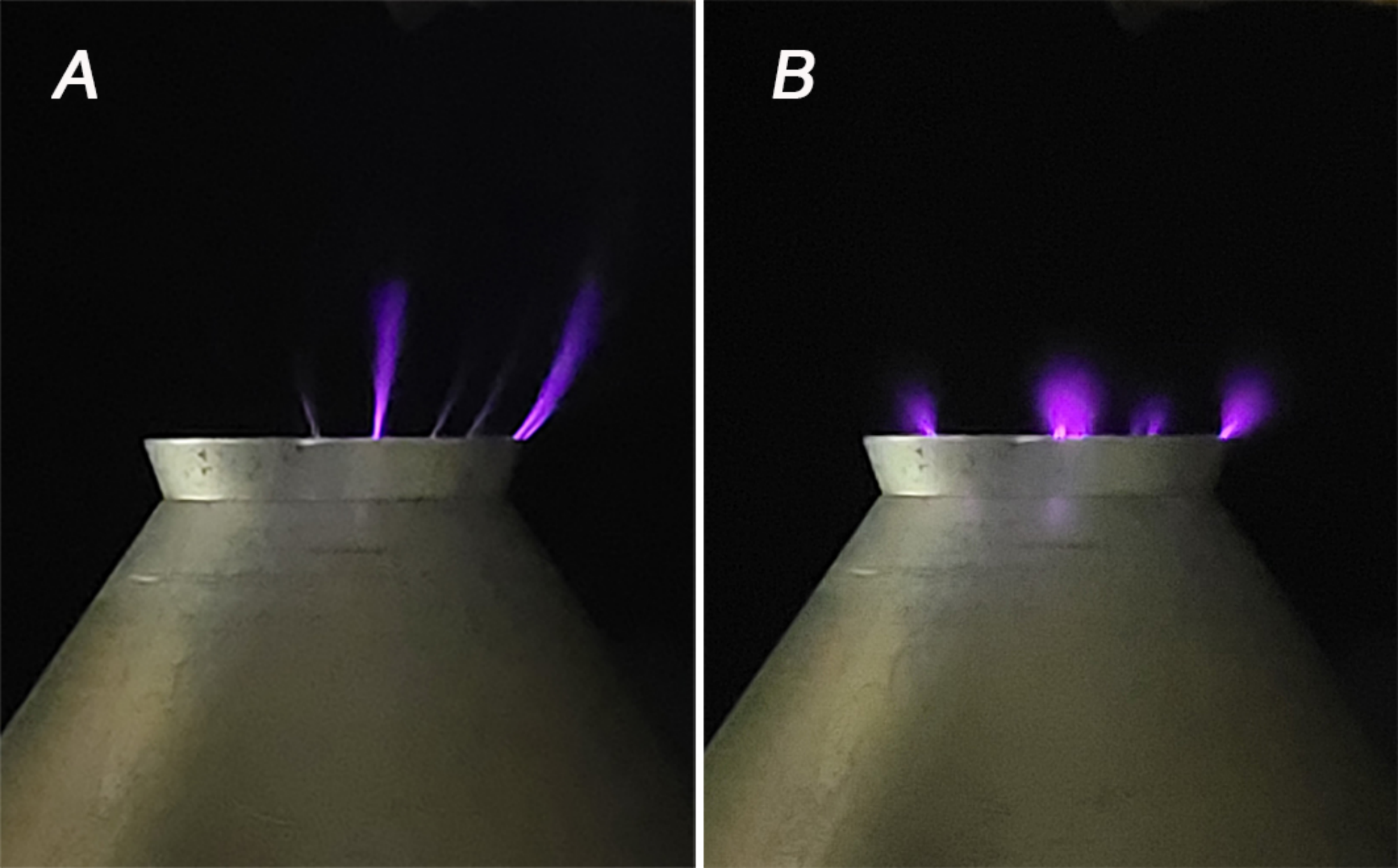
A
B

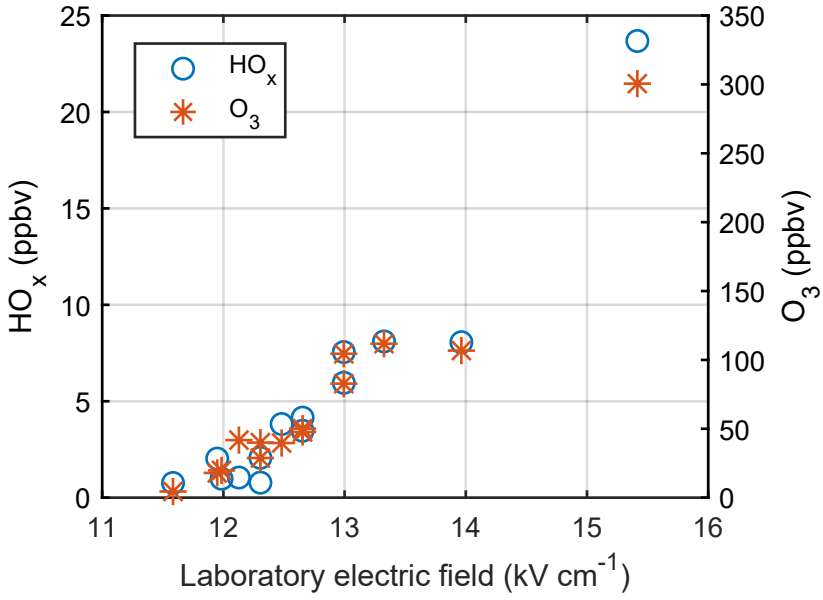
HO$_x$
O$_3$
HO$_x$ (ppbv)
O$_3$ (ppbv)
Laboratory electric field (kV cm^{-1})
0
5
10
15
20
25
0
50
100
150
200
250
300
350
11
12
13
14
15
16

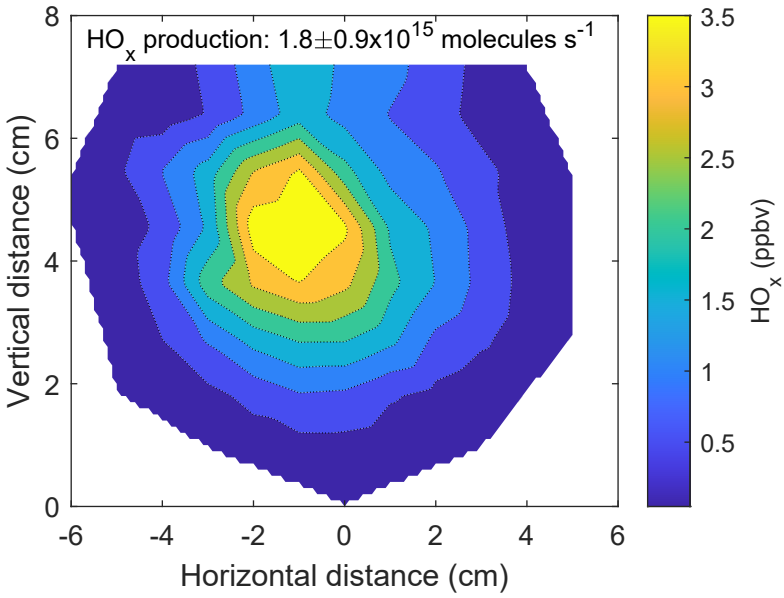
HO$_x$ production: 1.8±0.9x10^{15} molecules s^{-1}
Vertical distance (cm)
Horizontal distance (cm)
HO$_x$ (ppbv)
0
2
4
6
8
-6
-4
-2
0
2
4
6
0.5
1
1.5
2
2.5
3
3.5

PNAS
www.pnas.org

Supplementary Information for

Extreme hydroxyl amounts generated by thunderstorm-induced corona on grounded metal objects

William H. Brune*, Jena M. Jenkins, Gabrielle A. Olson, Patrick J. McFarland, David O. Miller, Jingqiu Mao, Xinrong Ren

William H. Brune
Email: whb2@psu.edu

This PDF file includes:

Supplementary text
Figures S1 to S9
Tables S1 to S2
SI References

Supplementary Information Text

1. TRAMP field study

The TexAQS II Radical Measurement Project (TRAMP) field study was conducted in Houston, TX in July and August, 2006. The goal of the study was to improve the understanding of the gaseous emissions and photochemistry that created the frequent air pollution in Houston, TX, particularly the ozone pollution (1). This site was chosen because it frequently sampled air from either downtown, the petrochemical facilities, or the cleaner air from the Gulf of Mexico to the south, and, because of its elevation, was less susceptible to nearby pollution sources. These months were chosen because peak ozone pollution occurs then.

A second study, the Study of Houston Atmospheric Radical Precursors (SHARP), occurred at the same location as TRAMP but in April and May 2009 (2). These months were chosen because plumes from biomass burning in Mexico and Central America reach Houston and a second annual ozone peak occurs then.

1.1. Ground-based Tropospheric Hydrogen Oxides Sensor (GTHOS) measurement

OH and HO_2 were measured with the Ground-based Tropospheric Hydrogen Oxides Sensor (GTHOS), which is extensively described in Faloona et al. (3). The basic technique is laser induced fluorescence in a low-pressure detection chamber. Air is pulled through a ~1 mm diameter orifice with a vacuum pump, producing a low-pressure (~5 hPa) flow into a pair of detection axis. A pulsed laser beam (3 kHz frequency, 20 ns long) is sent into multipass optical cells in each detection axis and is monitored at the exit of the cells. Microchannel plate detectors, set at right angles to the laser beam and the air flow, detect scattering from the laser pulse in low-gain mode and, after the laser pulse has ended, the weak OH fluorescence in high-gain mode. The laser is alternately tuned to a wavelength near 308 nm that is not absorbed by OH and then to one that is absorbed. The difference between these two signals is proportional to OH. Between the first and second detection axes, reagent NO is added, reacting with HO_2 to form OH, which is then detected. GTHOS was calibrated before, after, and during the study. The absolute uncertainty is $\pm$32%, 95% confidence and the limit-of-detection is 0.04 pptv for OH and 0.2 pptv for HO_2 for a one-minute averaging time.

The GTHOS electronic and laser were located in an air-conditioned trailer on the building roof and the GTHOS detection system was located at the northeastern corner of the scaffolding (Fig. S1A). During SHARP, the measurement of OH and HO_2 was made from the same scaffolding platform as during TRAMP, but the instrument was located 2 meters to the south, in the nearest corner in Fig. S1A. Electrical cables and fiber optics connected the electronics and the laser to the detection axes. The detection axis were housed in a weatherproof box, with the inlet extending 40 cm above the top surface of the box (Fig. S1B). A sonic anemometer was located ~2 meters to the east and ~20 cm below the GTHOS inlet.

The GTHOs inlet was higher than all structures except a triangular radio tower holding meteorology and photolysis frequency instruments. It was ~6 m to the southwest of the GTHOS inlet and ~3 m higher. It was topped with three brush-type lightning rods.

1.2. Evidence that the extreme OH and HO_2 are real

Two segments of the observed LHO_x provide tests of the validity of these extreme OH and HO_2 values (Fig. 2). As the laser wavelength was tuned on and off resonance with an OH absorption line, the signals were detected only when the laser wavelength was on resonance. However, being on or off resonance makes no difference to the scattering signal caused by rain drops entering the inlet, as can be seen in the off-resonance gap just after 17:59:30 in Fig 2B.

Two other diagnostics provide more evidence for these signals being real HO_2 and OH (Fig. 2C).

First, just before 15:32:00, the laser wavelength was scanned to ensure that measurements were being made with the $Q_1(2)$ transition in the $A^2\Sigma^+(v''=0) \rightarrow X^2\Pi^+(v'=0)$ OH electronic transition. The larger $Q_1(2)$ and smaller $Q_{21}(2)$ lines can be clearly seen, although their relative values are affected by the variability in the discharge-generated HO_x. Second, when the NO reagent to convert HO_2 to detectable OH is turned off from 15:30:30 to 15:31:00, the HO_2 values drop down to those expected of ambient OH detected in the HO_2 detection axis. These extreme signals are definitely due to HO_2 and OH.

Interferences for both HO_2 and OH can occur in environments with greater amounts of volatile organic compounds. The HO_2 interference involves the rapid internal conversion of organic peroxyl radicals to HO_2 after they react with the reagent NO used to convert HO_2 to detectable OH and is well understood (4). The OH interference appears to affect some OH detecting instruments more than others, with GTHOS, which was used in the TRAMP study, being one of the most sensitive (5). It occurs only in VOC-rich environments (4,5). While both interferences are now being minimized by instrument modifications, neither was for TRAMP or SHARP (6).

For these interferences to be responsible for the extreme OH and HO_2 observed under thunderstorms during TRAMP and SHARP, they would have to satisfy many criteria. First, they would have to produce, by two completely different mechanisms, hundreds of pptv to ppbv of OH and HO_2. The greatest OH and HO_2 interferences ever observed, even with a hundred ppbv of O_3 and hundreds of ppbv of VOCs, are a few pptv for OH and ~10 ppbv for HO_2. Second, the HO_2 interference mechanism is well-understood and has been successfully modeled when the initial VOCs are known (4). When the HO_2 interference is modeled for SHARP, even the most extreme of the hourly averages is less than 10 pptv (6).

Third, the OH interference was quantified with the addition of an OH-scavenging inlet during the second half of the SHARP study and was at most 0.5 pptv. After the scavenging inlet was added, no extreme OH was observed even under several thunderstorms of the same intensity as the one that caused extreme OH and HO_2 during the first half of SHARP. Fourth, since VOC-rich environments are shown to be necessary for the HO_2 and OH interferences, the observed extreme OH and HO_2 should correlate with VOCs in both the time series behavior, such as one-second spikes, and the variability. They do not. Fifth, we have been able to generate comparable amounts of extreme OH and HO_2 by electrical discharges in the laboratory and demonstrated that they cannot be due to interferences (7). The hypothesis that the extreme OH and HO_2 are caused by interferences fails to satisfy any of these criteria, lending more credibility that this extreme corona-generated OH and HO_2 is real.

2. Estimates of impact of corona-generated OH, O_3, and UV radiation on the atmosphere and surfaces

Extreme amounts of OH generated by corona can accelerate oxidation of atmospheric gases or of surface materials. The analysis of potential impacts rests on two conditions: the range of impact in time and space compared to that of ambient amounts of OH; the importance of OH oxidation compared to oxidation by other processes, particularly ultraviolet (UV) radiation and O_3 oxidation.

2.1. Range of impact

OH-producing corona are generated indoors by several devices, including electric motors, high-voltage equipment, and even increasingly used in building and residential air purification systems. They are also generated outdoors by lightning rods and other grounded metal objects under thunderstorms, such as is demonstrated in this paper, and by high voltage electrical power transmission lines and power distribution stations (8). Indoor impacts are the subject of ongoing research; here we focus on outdoor effects.

2.1.1. Comparison of corona-generated OH on lightning rods under thunderstorms to ambient OH

This comparison is between corona-generated OH molecules produced in a small volume around the lightning rod for a limited time when the thunderstorm is overhead to the total number of ambient OH molecules produced by well-known atmospheric photochemistry for a range of volumes and time periods. Comparison of the volume of air with the total number of ambient-produced OH molecules to the total number of corona-produced OH molecules is particularly important to determine the relative impact of corona-generated OH on atmospheric oxidation.

To find the total number of OH molecules that can contribute to atmospheric oxidation per lightning rod, we need to estimate the number of thunderstorms that create a corona on the lightning rod, the length of time and amount of OH produce for that time, and the fraction of that extreme OH that does not react with corona-generated HO_2 or OH and is thus available to react with other atmospheric constituents. In the United States east of the Rocky Mountains, approximately 50 thunderstorms occur over more than 100 cities annually (9). Based on the measurements presented in Fig. 1 of this paper, each thunderstorm produces, on average, 100 pptv of OH for ~400 s. From the laboratory studies and Fig. 5, this average value translates to a corona-generated OH production rate of 4×10^{14} molecules s^{-1}, of which a fraction of 35% will react with corona-generated HO_2 and OH, leaving 65% available to react in the atmosphere or on surfaces. This estimated total OH generated by corona on one lightning rod is 4×10^{18} molecules per year.

A typical ambient OH production rate per cm^3 of air is 10^7 molecules cm^{-3} s^{-1}, when averaged over a year. Its loss is due to the same gas-phase reactions that cause loss of corona-generated OH (excepting with corona-generated HO_2 and OH). By multiplying the ambient OH production rate per volume by the different ambient air volumes and times, we can produce a map of the ratio of total annual corona-generated OH to total ambient produced OH as a function of ambient OH volume and time (Fig. S6).

For shorter times and smaller volumes of ambient OH, the corona-generated OH is a million times more (lower left). Whereas for longer times and volumes, the contribution of corona-generated OH is negligible. The black line indicates the conditions for which corona-generated and ambient OH are equal. Of more interest is the time when the thunderstorms are generating corona, which is less than an hour total annually, marked by the red dashed line. The thunderstorm-induced corona-generated OH is greater than or equal to ambient total OH for ambient air volumes less than 100 m^3 and 1,000 times larger in a volume of 0.1 m^3. The most interesting case is the annual impact of corona-generated OH, which increases the oxidation by OH as much as a factor of 10 over ambient within 10 cm (volume = 0.01 m^3) of the lightning rod, thus greatly accelerating the degradation of nearby materials.

The same approach was applied to examine the potential impact of OH generated by corona on all lightning rods that might be in an urban area. Unfortunately, lightning rods are not required in most cities' building codes, so the only way to make an estimate is to assume that all buildings greater than 25 m (~6 stories) have lightning rods distributed every 6 m around the perimeter according to engineering guidance (10). Austin, TX is a rapidly growing mid-sized city and a good example of a typical urban area in a moderately lightning-prone area. According to the building data for 2013 (11), more than 400 buildings are taller than 25 m, requiring 1500 lighting rods to meet Underwriters Laboratories (UL) lightning protection guidance. For the Austin urban core with an area of ~5 km^2, to get the impact of corona-generated OH on the urban scale, we multiply the estimates for a single lightning rod by the estimated number of lightning rods.

These estimates for the urban scale indicate that the corona-generated OH impacts occur over a volume of 10^5 m^3 during the thunderstorms, and for a year, only over 20 m^3, which essentially is just near each lighting rod (Fig. S7). At the urban scale, given by the long dash line, the corona-generated OH is negligible for all time scales. In summary, impact of OH generated on lighting rods under thunderstorms is negligible for atmospheric processes on all scales greater than 1 m^3, but can provide greater than 10 times the oxidation as ambient OH for materials near the lightning

rods each year.

2.1.2. Comparison of corona-generated OH on HVTL to ambient OH

High-voltage electric power transmission lines (HVTLs) produce corona along the length of the lines and electrical power substations, where the the HVTL voltage is reduced for distribution to users (7). Research from the 1970's determined that 6×10^{17} O_3 molecules m^{-1} s^{-1} were generated for a 765 kV line in rainy or snowy weather (12,13). The amount of corona produced scales with the voltage and is as much as 10 times less in fair weather. We can scale these numbers to determine the amount of OH that is generated by typical HVTLs of ~270 kV in fair weather, which gives a typical O_3 production rate of 3×10^{16} O_3 molecules m^{-1} s^{-1}. From our paper, corona produce 28 O_3 molecules for each OH molecule, so that the OH production rate is estimated to be 1×10^{15} OH molecules m^{-1} s^{-1}. This value is consistent with the OH production rate measured in the laboratory for the GTHOS inlet (Fig. 5), giving us confidence in this estimate.

As was done in the previous case of lightning rods under thunderstorms, the corona-generated OH were compared to the ambient OH for different volumes and times, although in this case, the analysis was performed per meter of HVTL (Fig. S8). Unlike the cases of lightning rods under thunderstorms, the corona on the HVTL occur all the time, which is the reason that the line designating equal amounts of corona-generated and ambient OH is vertical on the plot.

Corona-generated OH equaling ambient OH occurs at a volume of 540 m^3 around and downwind of each meter of HVTL. For instance, for 1 m of HVTL, a plume 5 m high would have OH equal to or greater than ambient 100 m downwind. At a volume of 1 m^3 per meter of HVTL, corona-generated OH is over 500 times greater than ambient. In the 20 cm surrounding the HVTL, the exposure of the HVTL to OH is more than a 50,000 times that of ambient OH. Thus, corona-generated OH is a strong oxidizer of the materials near the HVTL.

Using a simple Gaussian plume model, we improve upon the plume estimate given above by comparing the downwind OH exposure along the plume centerline and comparing that to the ambient OH exposure. We assumed the atmosphere was moderately unstable (14) and the windspeed was 3 m s^{-1} perpendicular to the HVTL. The corona-generated OH exposure was calculated using MCMv3.3.1 in the F0AM framework constrained by conditions and model parameters appropriate for a slightly polluted forest (OH reactivity: 5.5 s^{-1}; NO: 0.47 ppvb; NO_2: 0.8 ppbv) and then dispersed according the the Gaussian plume equation for a line source (15).

The centerline plume corona-generated OH is more than 10^{10} OH cm^{-3} at the HVTL and does not become equal to the ambient OH until the plume is 100 m downwind. The clearance on either side of HVTLs is typically less than 25 m, which means that structures or trees at the edge of the right-of-way and the height of the HTVLs are receiving more than 10 times the ambient OH amounts continually. For stronger winds or stable conditions, this continual dosing of the nearby forest or structures increases this OH exposure to 100 times ambient. These estimates of impact do not include the possible impact of air that has flown past the corona, been oxidized, and, as a result, has a different chemical composition.

2.2. Comparison of impact of OH, O_3, and UV on commonly used insulating materials

In the absence of corona-generated OH, degradation of materials is driven more by solar UV radiation than by ambient OH levels, which are a diurnally averaged 1-4×10^6 molecules cm^{-3}. A substantial amount of research has been conducted on this solar UV degradation and chemical degradation sequences have been developed and refined (16). They are all initiated by solar UV below~360 nm wavelength, but, as part of the sequence, OH is produced and participates in the degradation. Ozone can also play a role, but only if the polymer material has exposed double carbon bonds.

Polymers are formulated to be resistant to solar UV. This UV resistance for some more UV-susceptible polymers is being achieved by adding UV-blocking or absorbing chemicals, or by adding other chemicals that interrupt the reactive chemistry that causes the polymer decomposition (17). For use as HVTL and power substation insulators, two polymers have emerged as having the necessary mechanical properties and resistance to degradation by solar UV and O_3: Ethylene propylene diene monomer (EPDM), and polydimethylsiloxane (PDMS). However, even these polymers degrade in sunlight, albeit much slower rate than others (18).

The polymers are also degraded by nearby corona more rapidly than expected (19). Degradation results in loss of hydrophobicity, increased electrical conduction, and mechanical failure with cracking and chalking. It is always assumed that corona-generated UV is involved, with possible contributions from corona-generated O_3, although OH inevitably is produced in the oxidation process and participates in further degradation. OH directly produced by the corona appears to have never been considered. The question is "Is the corona degradation of these polymers initiated by UV radiation, O_3, or OH?"

From the laboratory studies of corona presented in this paper and another paper (21), we can determine relative importance of these three. EPDM (SMILES chemical formula: C=CC1=CC2CC1CC2=CCC=CC) has three double bonds in each monomer unit, and is thus susceptible to attack by UV radiation, O_3, and OH. However, the corona-generated O_3-to-OH ratio is only 28, while the the reaction rate coefficients for the gas-phase alkene is in the range of 10^{-11} cm^3 $molecule^{-1}$ s^{-1} for OH and 10^{-17} cm^3 $molecule^{-1}$ s^{-1} for O_3. Thus, degradation initiation is 30,000 times faster by OH than by O_3. PDMS (SMILES chemical formula: C[Si](C)(Cl)Cl, CO[Si](C)(C)OC) has no double bonds and thus no reaction with O_3. The reaction rates of OH with organosilicons is ~10^{-12} cm^3 $molec^{-1}$ s^{-1} (21), so reactions on surfaces should be fast and the uptake coefficient should be close to 1, making diffusion to the surface the rate-limiting step in the OH attack on these polymers. For these and all other polymers, corona-generated OH is the dominant degradation initiator and corona-generated O_3 is negligible.

How do the corona-generated UV flux and OH flux compare? From our laboratory studies (22), corona generate an OH production rate of 3×10^{14} molecules s^{-1} for a UV flux of 5×10^5 photons cm^{-2} s^{-1} for wavelengths < 200 nm at a distance of 22 cm. We can scale both this UV flux and this OH production rate to determine the UV flux and the OH flux close to the corona (~1 cm) so that they can be compared.

For the OH flux, scaling data from two laboratory studies can be used to produce the estimate. The OH production rate in Fig. 5 has a peak HO_x mixing ratio of 3.5 ppbv, of which 1.7 ppbv is OH, with an OH production rate of 2×10^{15} OH s^{-1}. In a separate study (22), the OH production rate is compared to UV flux. For a UV flux that will be discussed in the next paragraph, the OH production rate was 3×10^{14} OH s^{-1}. Thus, the peak OH mixing ratio that corresponds to the OH production rate for the measured UV flux is $(3\times10^{14}/2\times10^{15})$ $(1.7)(2.4\times10^{10}) = 6\times10^9$ OH cm^{-3}. Assuming that the insulator is a cylinder of diameter 5 cm, we can use the derivation of molecular flux to or from a cylindrical surface (23) to estimate the OH flux to the surface. It is 1.4×10^{10} OH cm^{-2} s^{-1}.

For the UV flux, the OH production rate of 3×10^{14} OH s^{-1} corresponded to a corona UV flux in the 180-200 nm wavelength band of 5×10^5 photons cm^{-2} s^{-1}, at a distance of 22 cm (22). This photomultiplier detection was calibrated against a NIST-calibrated Si photodiode. Scaling this number to 2 cm from the corona, which was the distance used to find the OH flux, gives 6×10^7 photons cm^{-2} s^{-1}. The measured UV flux in the 180-260 nm band was 1.5×10^9 photons cm^{-2} s^{-1} and for the 180-290 nm band was 6×10^9 photons cm^{-2} s^{-1}. The total UV corona flux in the 300-350 nm band is several hundred times greater (23).

The OH and UV radiation fluxes are the same order of magnitude. It is not yet clear if these flux values are appropriate for corona on HTLVs, so they must be scaled once that information is

available. However, our laboratory studies show that they do scale together so that their relative value remains the same. Thus the following discussion will apply no matter how the amount of corona on HVTLs differs from our laboratory results.

Consider first a surface made of EPDM. Some of its C-C and C-H bonds can be broken by UV radiation at wavelengths less than ~350 nm, while most require radiation wavelengths less than 280 nm (25). Thus, corona-generated UV radiation can be responsible for EPDM degradation. OH readily reacts with ethylene and propylene in the gas-phase so that OH can also be responsible for EPDM degradation. However, the environmental degradation of EPDM is most likely initiated by solar UV radiation, with corona-generated UV radiation and OH playing a secondary role, because the solar UV flux in the 300-350 nm range (~10^{15} photons cm^2 s^{-1}) is orders of magnitude larger than either the corona-generated UV flux or the OH flux.

Surfaces made of PDMS have been shown to be more resistant to degradation, including by UV radiation (20), which is one reason that PDMS is a polymer of choice for HVTL applications. This result is consistent with the stability of gas-phase organosilicon compounds under 20 minutes of maximum simulated solar radiation in an environmental chamber (21). The most exposed bonds in PDMS – the Si-O and H_2C-H bonds – require radiation wavelengths less than 260 nm for photodissociation. Thus, solar UV radiation is less effective for PDMS degradation than it is for EPDM degradation.

The appropriate UV flux for corona-generated UV less than 260 nm is 1.5×10^9 photons cm^{-2} s^{-1}, which is less than the simultaneous OH flux of 6×10^9 molecules cm^{-2} s^{-1}. Both UV radiation and OH initialize PDMS degradation by removing an H from a methyl group (16,21). After the H is abstracted, whether it be by UV radiation or OH reaction, the resulting degradation sequence leads to insulator failure (16).

For PDMS, the solar UV flux is negligible below 290 nm, so that the corona-generated UV flux and OH flux can be more important than solar UV flux for PDMS degradation. Since these two fluxes are the same order of magnitude, more information on the efficiency of each flux removing an H from the methyl groups is required to know whether corona-generated UV radiation or OH is more important. Several research studies have described PDMS degradation in detail, but we have not found one that quantifies the mechanism of photodissociation. Further, we found no studies that even mention that corona-generated OH might be involved, even though corona-generated OH is known to scientists developing methods to remove environmental pollution (26). The modeling or laboratory experiments to quantify the surface chemistry involving corona-generated UV radiation and OH, so that their relative importance can be compared, is well beyond the scope of this paper. However, the analysis presented here demonstrates that corona-generated OH is more likely to degrade PDMS and other polymers than corona-generated UV radiation is.

2.3. Uncertainty estimates for these impact calculations

The uncertainty of these estimates of the impact of corona-generated OH are based on our observations during TRAMP and SHARP on the GTHOS inlet and on our recent laboratory studies. All uncertainty estimates are given in terms of multiplicative factors and are at 68% confidence.

For the lightning rods, we estimate the following uncertainties as multiplicative factors: number of thunderstorms: 1.3; corona duration: 1.3; coronal OH production: 1.5; fraction reacting with corona-generated HO_2: 1.3; and annual ambient OH production: 2. The total uncertainty for the corona-to-ambient OH is a factor of 2.6, which we round up to 3 to account for unknown unknowns. For urban scale, our estimate of the uncertainty for total number of lightning rods in a mid-sized urban area is a factor of 3, giving the total uncertainty for ratio of corona-to-ambient OH of a factor of 4.2.

For the high-voltage electrical power transmission lines (HVTLs), we estimate the following uncertainties: ozone production: 3; O_3 to OH scaling: 1.3; ambient OH concentration: 2. The total uncertainty for HVTL corona-to-ambient OH is a factor of 3.6, which we round up to 4 to account for unknown unknowns.

For surface oxidation and degradation, we estimate the following uncertainties for the OH flux: OH concentration: 2; boundary layer thickness: 2; number of exposed methyl groups: 3. The total uncertainty estimate in the rate of surface oxidation initiated by corona-generated OH is 4.1. For the corona UV flux at wavelengths below 200 nm, we estimate the following uncertainties as multiplicative factors: 187 nm flux: 2; ratio 200-300 nm flux to 187 nm flux: 4; scaling flux to a nearby surface: 2. The total uncertainty estimate in the corona UV flux is a factor of 5. We have no way to estimate the uncertainties for detailed mechanisms for the degradation initiation by corona-generated UV radiation or OH.

These uncertainty estimates are all in the range of a factor of 4 to 5 at 68% confidence. There are also unknown uncertainties associated with applying these uncertainty estimates to other locations and times. Planned laboratory and field measurements will cut these uncertainty estimates substantially.

3. Data access

The data sets and information on the modeling code used in this study are publicly available at: https://doi.org/10.26208/k4ce-zw19

3.1. TRAMP measurement files

1 file: TRAMP_merge_meas_mod_version20211230.csv

The merge of 1-minute data from all TRAMP measurements for all times is a csv file..
The header gives the name of the variable and its units. Note that the extreme values for observed OH and HO_2 have been removed. The merge also contains the OH and HO_2 modeled with RACM (S4). "-9999" indicates no measurement. These data were used to plot Fig. 1C and 1D.

18 files: TRAMP_2006MMDD_version_20211211.csv

The merges of 5-Hz data from TRAMP measurements for only a few hours around the times of the extreme OH and HO_2 are csv files. MMDD is the month and day that the file record starts, but each file typically runs from morning of the first day to the morning of the next day. The header gives the names of the variables and their units. TRAMP measurements in the 1-minute merge are interpolated to 5-Hz. In addition to these measurements and the 5-Hz OH and HO_2 measurements, are the following variables:

- GTHOS_Cal: "1" indicates an hourly period of instrument testing that started at 30 minutes past each hour.
- GTHOS_OHRay: Counts/0.2s is the OH scattering signal caused by rain entering the GTHOS inlet.
- GTHOS_OnLine: "1" indicates times when the laser wavelength is tuned to the OH absorption line enabling the measurements of OH and HO_2. "0" indicates background measurements.
- GTHOS_Scan: "1" indicates periods when the laser wavelength is being scanned, producing the OH spectrum around the line that is being used.

"-9999" indicates no measurement.

3.2. Cloud and weather information

2 GOES movies of Infrared Water Vapor and Visible for Houston area

The two avi files contain movies of the Houston area. Intermixed are the Infrared Water Vapor and the Visible channels. The dates covered in each file are listed in the file name. These data are used in Table S1.

GOES_IRWV_Vis_819_822_823_911_915_916_917_924.avi
GOES_IRWV_Vis_826_827_901_902_910

3.3. Surface weather data from the NWS site, William Hobby Airport, can be found at the following website: https://www.weather.gov/wrh/Climate?wfo=hgx

The following settings were used to retrieve the data:

Location: Houston, William, TX
Date: first 2006-8; second 2006-9
Product: Daily data for a month

3.4. Photochemical Box Modeling

The code for the photochemical box modeling can be best obtained from https://github.com/AirChem/F0AM, a site maintained by Glenn Wolfe. The code is based on Matlab, so the reader will need to have access to Matlab..

Model parameters were set as follows:

kdil = 10^{-12} ; % Hz
ModelOptions.Verbose = 1;
ModelOptions.EndPointsOnly = 0; % we want the calculations as a function of time
ModelOptions.LinkSteps = 0;
ModelOptions.Repeat = 1;
ModelOptions.IntTime = 120; % seconds
ModelOptions.TimeStamp = 0.0;

The input files to run the 17 different cases are in the file TRAMP_photochemical_box_model_inputs.csv.
The chemical mechanism was MCM v331.

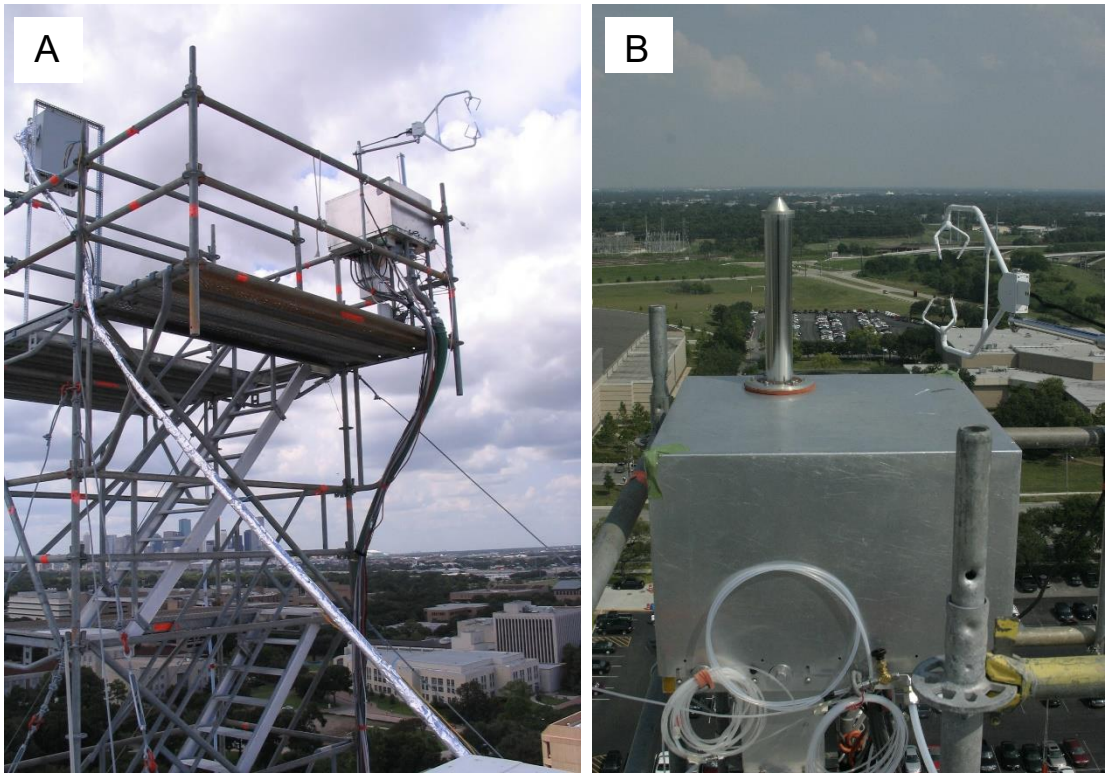

Figure S1. GTHOS on top of Moody Tower I during TRAMP in 2006. (A) The GTHOS sampling inlet was 5 m above the roof surface on construction scaffolding and located in the northeast corner of the scaffolding, which was at the north edge of the building. The sonic anemometer was oriented to the east (90^{o}). (B) The GTHOS sampling inlet (5.5 cm dia.) is 40 cm above the flat surface of the GTHOS detection system. Nearby vertical structures include the extension tubes for the scaffolding and the sonic anemometer, although the GTHOS inlet was higher than all of them.

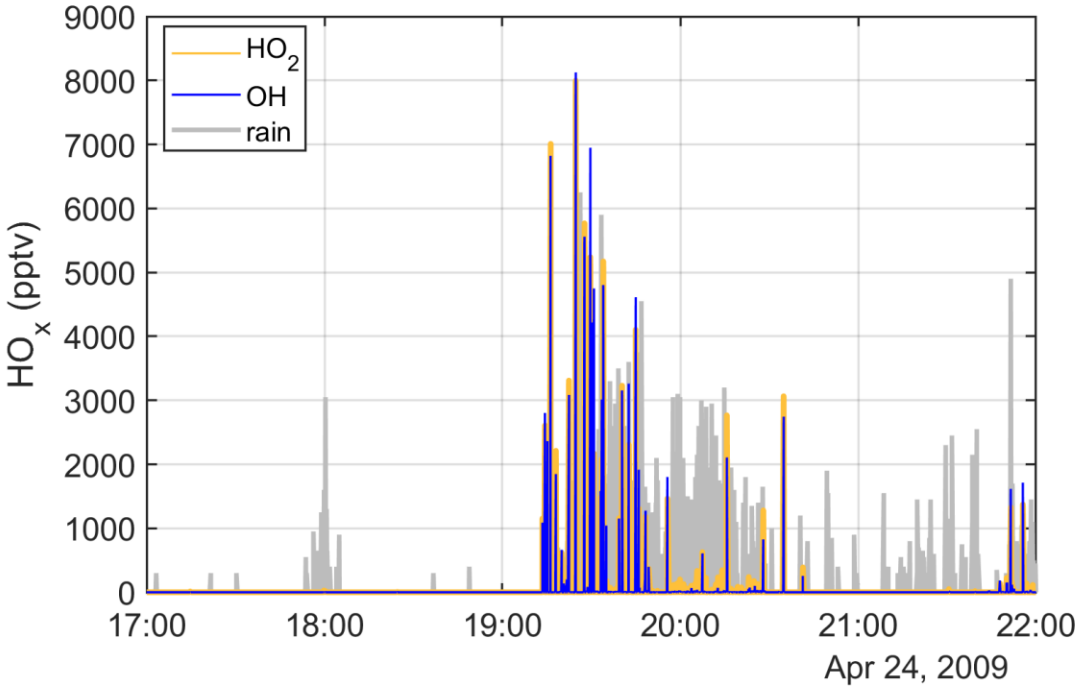

Figure S2. Enhanced HO_x observed during the 2009 SHARP study. HO_2 (gold), OH (blue), and scattering indicating rain (gray) all consist of individual 0.2 s spikes. HO_2 and OH spikes always coincide and these spikes rarely coincide with the OH Rayleigh scattering spikes.

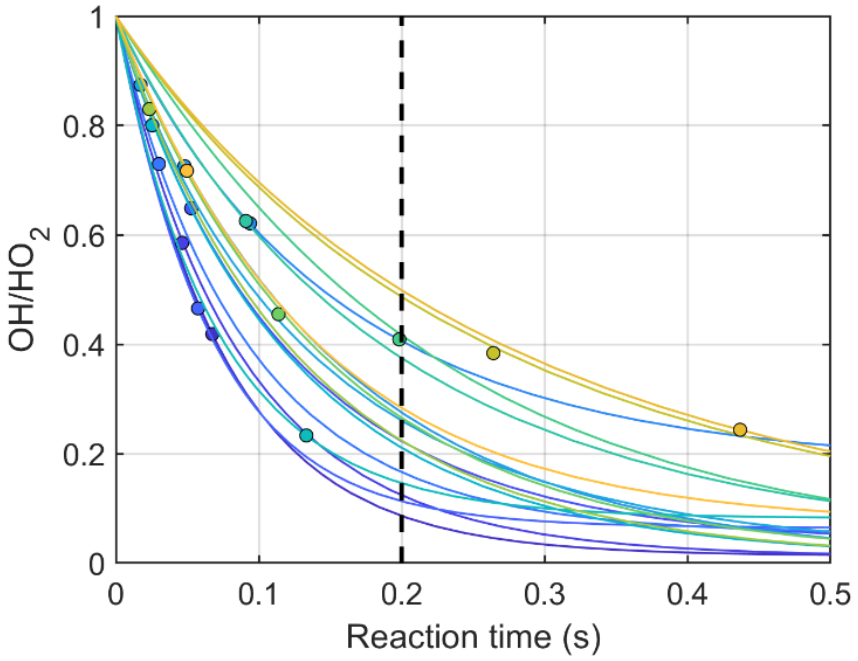

Figure S3. Modeled change in OH/HO_2 for 17 LHO_x spikes during TRAMP. Lines are the modeled ratios as a function of time, assuming $[OH]=[HO_2]$ initially. Dots are the measured ratios of the LHO_x spikes. Fifteen are achieved in less than 0.2 seconds, which is the time resolution of the measurements. The different colors indicate whether the measurements were early (cooler color) or late (warmer color) in the field study.

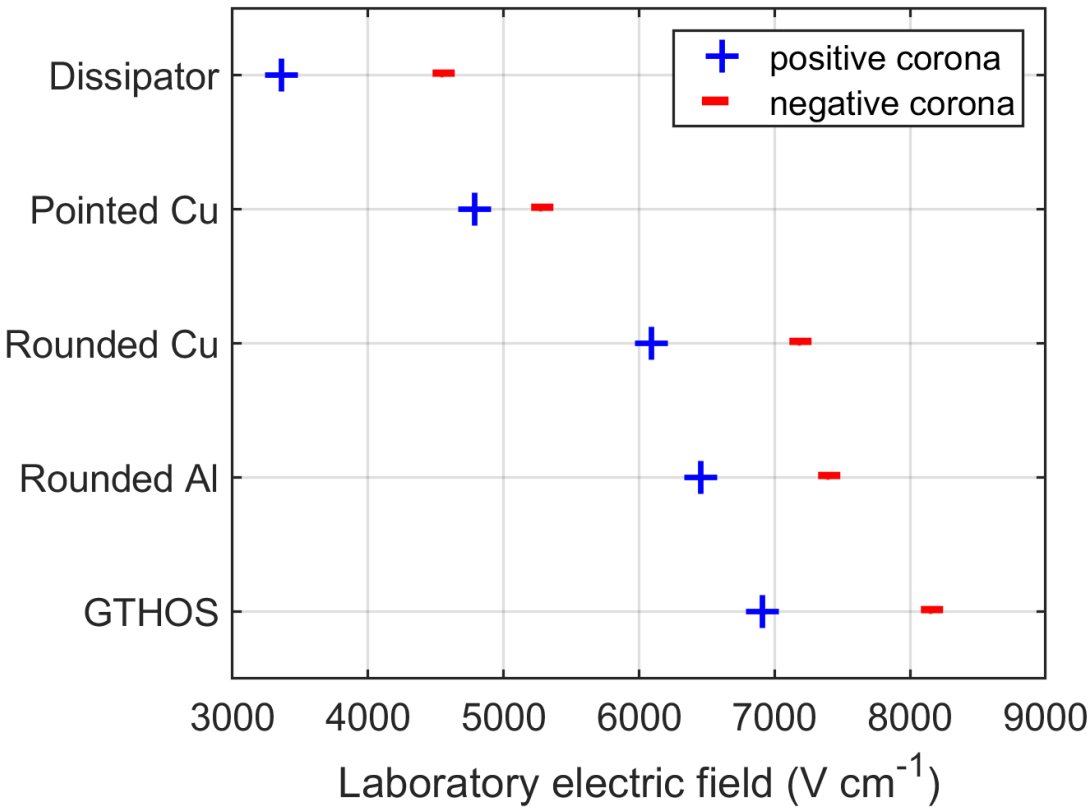

Figure S4. Electric field required to initiate coronas for different electrodes. The electrodes are a static dissipator, pointed copper lightning rod, rounded copper lightning rod, rounded aluminum lighting rod, and the GTHOS inlet. The same trends hold for positive (+) and negative (-) coronas.

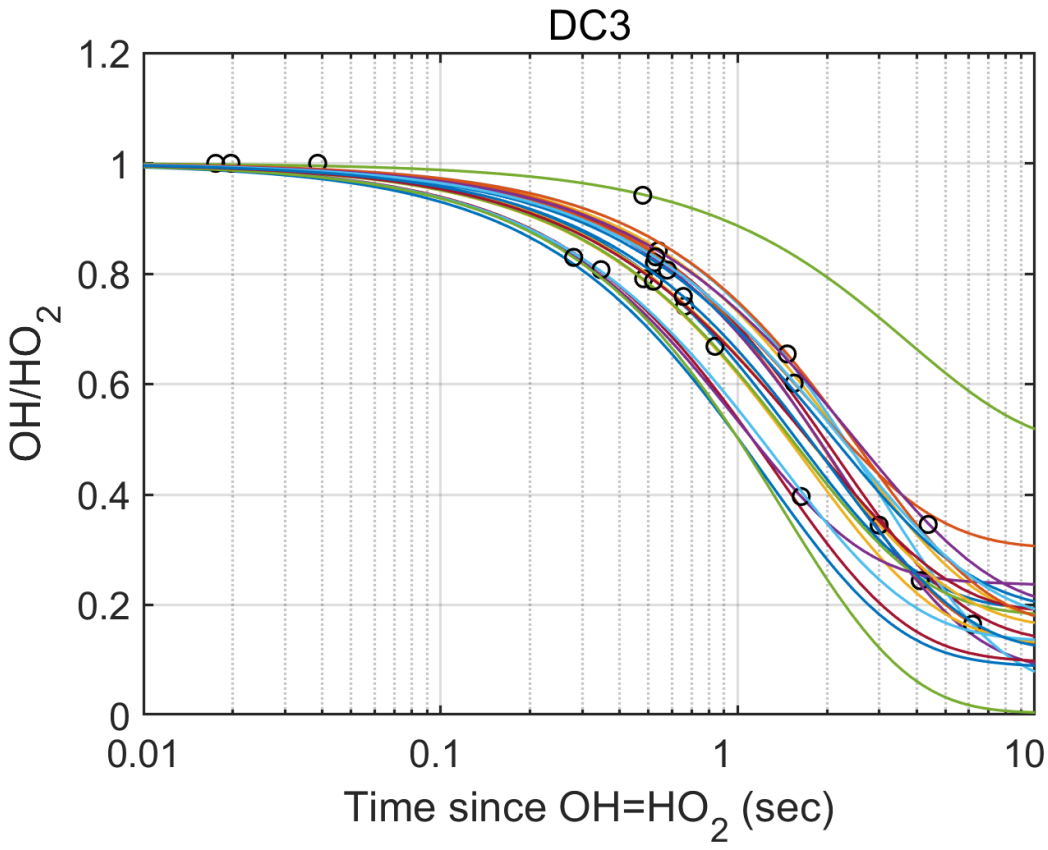

Figure S5. Modeled change in OH/HO_2 for 22 LHO_x spikes during DC3. Lines are the modeled ratios as a function of time, assuming $[OH]=[HO_2]$ initially. Open circles are the measured ratios of the LHO_x spikes. The different colors indicate whether the measurements were early (blue) or late (yellow) in the field study. Nineteen encounters occur more than 0.2 seconds after the electrical discharge occurred, with the median time of 0.56 seconds.

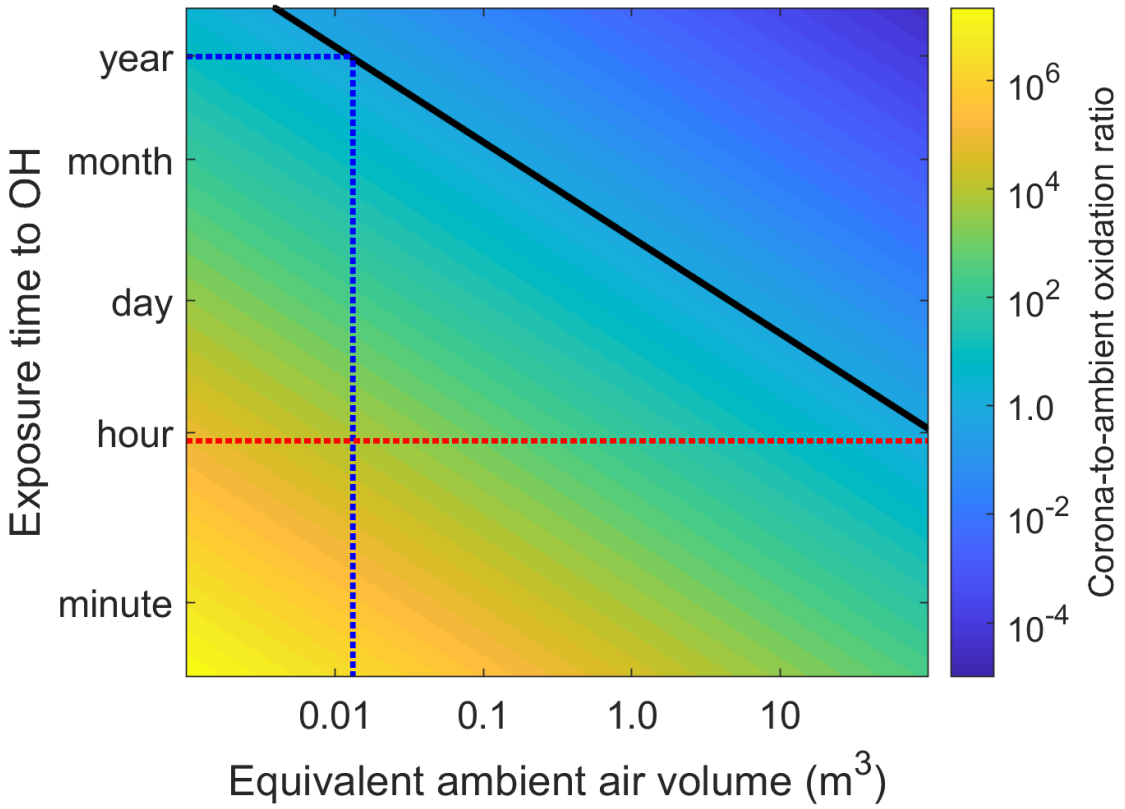

Figure S6. Comparison of corona-to-ambient ratio of total OH molecules for one lightning rod during a total of 50 storms. The total number of OH molecules produced during the storms by corona in the small corona volume can be compared to the total number of OH molecules produced in different air volumes and for different times. At small volumes and short times (lower left), corona produce much more OH than ambient conditions. The ambient and corona OH become equal (black line). At larger volumes and times (upper right), OH from corona are insignificant compared to ambient OH. During the storms, corona-produced OH is greater than ambient OH produced in 100 m^3 of air (red dotted line), but on and annual basis, is greater only near the lightning rod (blue dotted line).

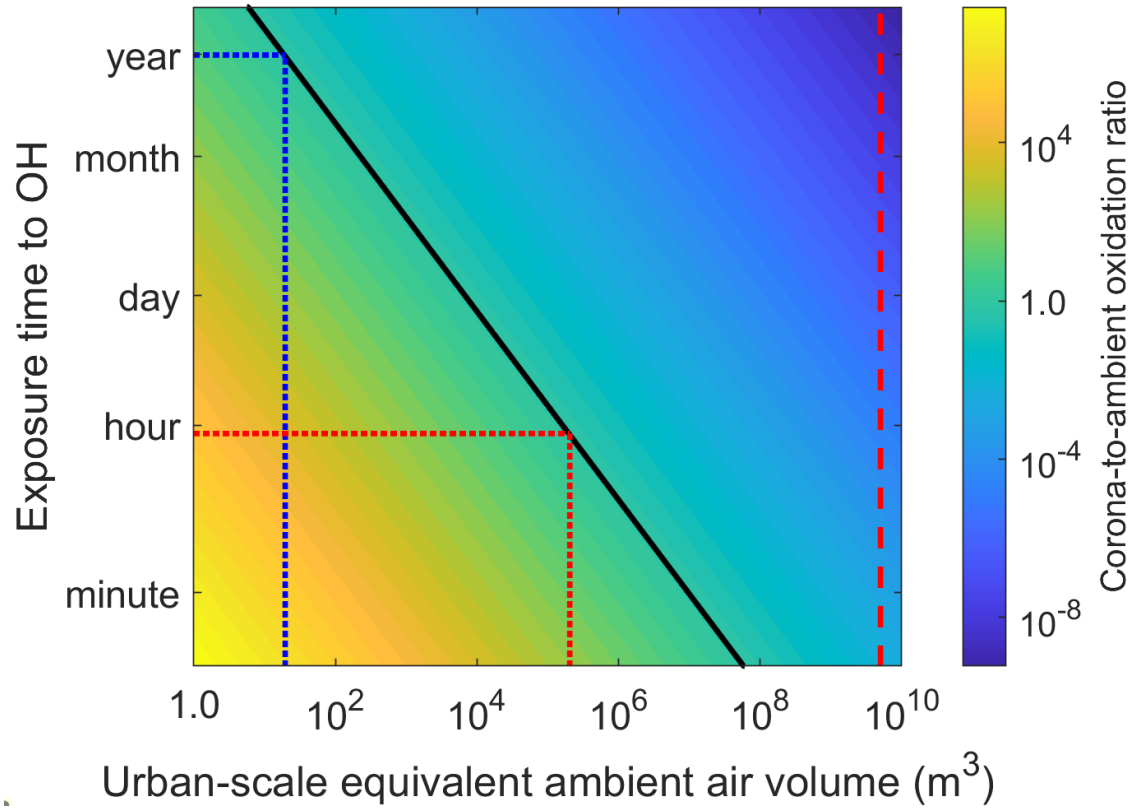

Figure S7. Comparison of corona-to-ambient ratio of total OH molecules for all lightning rods n a mid-sized urban center under 50 storms. The total number of OH molecules produced during the storms by corona in the small corona volume can be compared to the total number of OH molecules produced in different air volumes and for different times. At small volumes and short times (lower left), corona produce much more OH than ambient conditions. The ambient and corona OH become equal (black line). At larger volumes and times (upper right), OH from corona are insignificant compared to ambient OH. During the storms, corona-produced OH is greater than ambient OH produced in 100 m^3 of air (red dotted line), but on an annual basis, is greater only near the lightning rod (blue dotted line). The air volume for the urban center is the dashed red line.

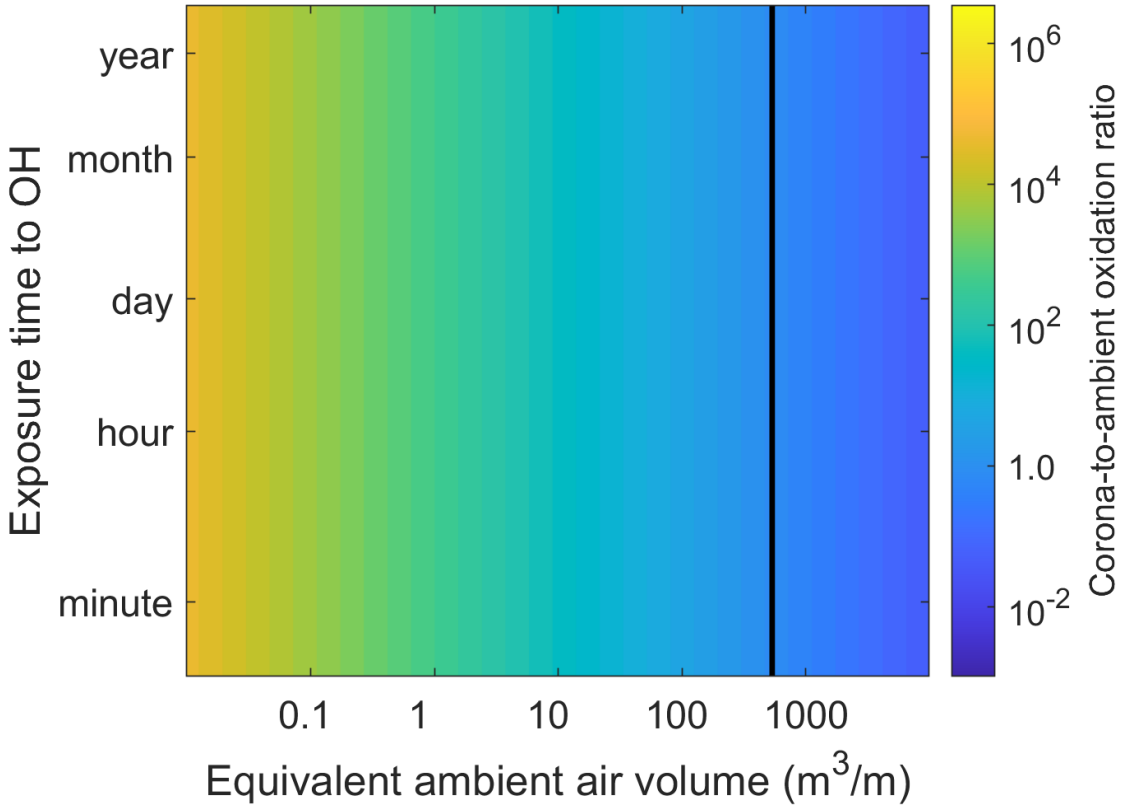

Figure S8. Comparison of corona-to-ambient ratio of total OH molecules for continuous corona on a high-voltage electrical power transmission line (HVTL) per meter of line. The total number of OH molecules produced by corona in the small corona volume on and downwind of the HVTL can be compared to the total number of OH molecules produced in different air volumes and for different times. For smaller volumes (left), corona produce much more OH than ambient conditions. The ambient and corona OH become equal (black line). At larger volumes (right), OH from corona are insignificant compared to ambient OH.

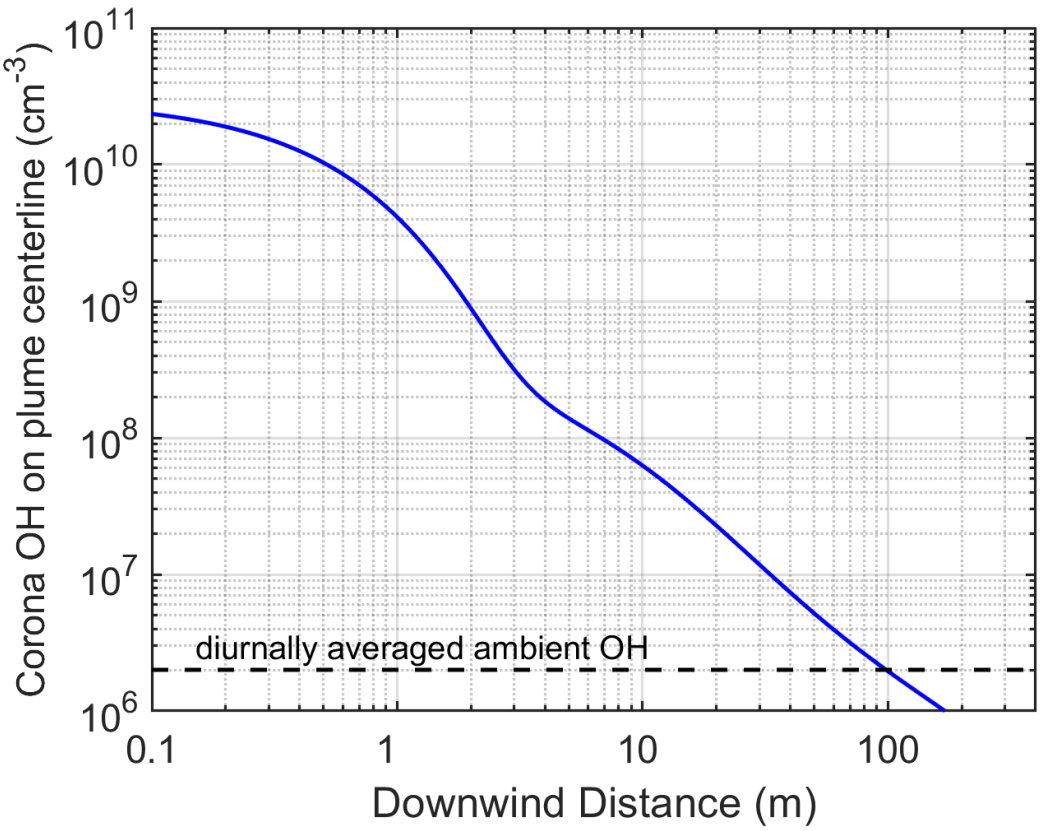

Figure S9. Centerline OH concentration in a Gaussian plume downwind of corona along a high-voltage electrical power transmission line. Corona-produced OH decay is due to both chemistry and dispersion. Assumed was a windspeed of 3 m s^{-1} and Pasquill dispersion class of moderately unstable. Corona-produced equals ambient OH at 100 meters downwind, where the Gaussian dispersion vertical standard deviation is ~10 m.

	Hobby Airport[1]					
Date	Rain total (in)	LHO_x time (GMT = CST + 6 hours)	OH Rayleigh scattering time (GMT)	overhead cloud brightness T (K±5K)	cloud type Cb: cumulonimbus Sc: stratocumulus	enhanced HOx behavior[2]
11-18 Aug	0					
19-Aug	1.93	13:38-14:18 15:48-16:00	13:55-14:11 15:39-16:00	195; 205	extensive Cb; Cb	spikes; spikes
20-21 Aug	0	0	0			
22-Aug	0	0	21:01-21:20	235	edge of small Cb	
23-Aug	0.16	17:52-19:24	18:20-21:38	205	persistent Cb	spikes
24-25 Aug	0	0	0			
26-Aug	Trace	0	17:18-17:46	225	edge of small Cb	
27-Aug	0.02	0	17:11-17:25	220	line of small Cbs	
28-31 Aug	0	0	0			
1-Sep	Trace	23:58-24:00	23:55-24:00	215	Cb	variable continuum
2-8 Sep	0	0	0			
9-Sep	0.09	0	0			
10-Sep	0.23	21:44-22:30	21:30-22:30	225	small Cb	weak spikes
11-Sep	0.08	19:43-19:49	19:12-20:26 22:13-24:00	215	Cb	weak spikes then variable continuum
12-Sep	0.01		0			
13-14 Sep	0		0			
15-Sep	0.77	21:07-21:45	20:40-22:00	205	Cb	variable continuum
16-Sep	0	0	21:50-22:30	230	small Cb to north	
17-Sep	0.59	0	14:24-14:53 17:24-17:35	220	widespread Sc	
18-Sep	0.06	0	0			
19-22 Sep	0	0	0			
23-Sep	0.78	0	0			
24-Sep	0.47	4:17-8:43	4:40-11:45	195	widespread large Cbs	spikes, then continuum; then spikes
25-28 Sep	0	0	0			

[1] Hobby Airport located 9.4 km southeast of the site
[2] Spikes are short enhancements (e.g., Fig 2A); variable continuum is longer unsteady enhancements (e.g., Fig. 2B and 2C).

Table S1. Weather and times with LHO_x and GTHOS Rayleigh scattering for TRAMP.

Measurements used to constrain the photochemical box model			
Environment	**Inorganics**	**VOCs**	**VOCs**
Pressure	O_3	HCHO	Ethene
Temperature	NO	CH_3OOH	Propene
Water vapor	NO_2	Acetaldehyde	Butenes
Photolysis frequencies	CO	Ethane	Pentenes
	HNO_3	Propane	Hexenes
	HOOH	Butanes	Benzenes
		Pentanes	Xylenes
		Hexanes	Toluenes
		Acetylene	Isoprene

Table S2. Measurements used to constrain the photochemical box model

SI References

1. B. Lefer, B. Rappenglück, J. Flynn, C. Haman, Photochemical and meteorological relationships during the Texas-II Radical and Aerosol Measurement Project (TRAMP). Atmos. Environ., 44, 4005-4013, doi:10.1016/j.atmosenv.2010.03.011 (2010).

2. E. Olaguer, C. Kolb, B. Lefer, B. Rappenglück, R. Zhang, J. Pinto, Overview of the SHARP campaign: Motivation, design, and major outcomes. *J. Geophys. Res. Atmos.*, 11,. 2013JD019730. 10.1002/2013JD019730 (2014).

3. I. C. Faloona, D. Tan, R. L. Lesher, N. L. Hazen, N. L., C. L. Frame, J. B. Simpas, et al., A laser-induced fluorescence instrument for detecting tropospheric OH and HO_2: Characteristics and calibration. *Journal of Atmospheric Chemistry,* 47, 139-167. doi:10.1023/B:JOCH.0000021036.53185.0e (2004).

4. H. Fuchs, B. Bohn, A. Hofzumahaus, F. Holland, K. D. Lu, S. Nehr, F. Rohrer, A. Wahner, Detection of HO2 by laser induced fluorescence: calibration and interferences from RO_2 radicals, *Atmos. Meas. Tech.*, 4, 1209–1225, doi:10.5194/amt-4-1209-2011 (2011).

5. J. Mao, X. Ren, L. Zhang, D. M. Van Duin, R. C. Cohen, R. C., Park, J.-H., Goldstein, A. H., Paulot, F., Beaver, M. R., Crounse, J. D., Wennberg, P. O., DiGangi, J. P., Henry, S. B., Keutsch, F.N., Park, C., Schade, G. W., Wolfe, G. M., Thornton, J. A., Brune, W. H. Insights into hydroxyl measurements and atmospheric oxidation in a California forest,

6. X. Ren, D. van Duin, M. Cazorla, S. Chen, J. Mao, L. Zhang, W.H. Brune, J.H. Flynn, N. Grossberg, B. L. Lefer, B. Rappenglück, K.W. Wong, C. Tsai, J. Stutz, J.E. Dibb, B.T. Jobson, W.T. Luke, and P. Kelley, Atmospheric oxidation chemistry and ozone production: Results from SHARP 2009 in Houston, Texas, *J. Geophys. Res.*, **118**, 5770–5780, DOI: 10.1002/jgrd.50342 (2013).

7. J. M. Jenkins, W. H. Brune, D. O. Miller, Electrical Discharges Produce Prodigious Amounts of Hydroxyl and Hydroperoxyl Radicals. *J. Geophys. Res.*, 10.1029/2021JD034557 (2021).

8. J. G. Anderson, M. Baretsky, D. D. MacCarthy, Corona-loss characteristics of EHV transmission lines based on Project EHV Research, *IEEE Trans. Power Apparatus and Systems*, PAS-85, 1196-1212. (1966)

9. United Nations Statistics Division, UNdata, Available at https://data.un.org Deposited 30 March 2022.

10. UL, Lightning Protection and Application Guide, website: https://code-authorities.ul.com/wp-content/uploads/2014/04/LightningProtectionAG.pdf Deposited 7 April, 2022.

11. City of Austin, TX, https://data.austintexas.gov/Locations-and-Maps/Building-Footprints-Year-2013/7bns-7teg Deposited 7 April 2022.

12. J. F. Roach, F. M. Dietrich, V. L. Chartier, H. J. Nowak, Ozone concentration measurements on the C-line at the Apple Grove 750 kV Project and theoretical estimates of ozone concentrations near the 765 kV lines of normal design, *IEEE Trans. Power Apparatus Systems*, PAS-97, 1392-1401, (1978).

13. S. A. Sebo, J. T. Heibel, M. Frydman, C. H. Shih, Examination of ozone emanating from EHV transmission line corona discharges, *IEEE Trans. Power Apparatus Systems*, PAS-95, 693-702, (1976).

14. J. H. Seinfeld, S.N. Pandis, *Atmospheric Chemistry and Physics,* (John Wiley and Sons, 1998), pp 929-931.

15. J. G. Droppo, Field determinations of HVDC ozone production rates, *Pacific Northwest Laboratory*, CONF-7904144-1 (1979).

16. M. P. Kroonblawd, N. Goldman, A. Maiti, J. P. Lewicki, Polymer degradation through chemical change: A quantum-based test of inferred reactions in irradiated polydimethylsiloxane, *Phys. Chem. Chem. Phys*, 24, 8142-8157, DOI: 10.1039/d1cp05647f (2022).

17. E. Yousif, R. Haddad, Photodegradation and photostabilization of polymers, especially, polystyrene: Review, *SpringerPlus*, 2:398 (2013).

18. R. Sudararajan, A. Mohammed, N. Chaipanit, T. Karcher, Z. Liu, In-service aging and degradation of 345 kV EPDM transmission line insulators in a coastal environment, *IEEE Trans. Dielectrics Elect. Insulation*, 11, 348-361 (2014).

19. Y. Zhu, K. Haji, M, Otsubo, C. Honda, Surface degradation of silicone rubber exposed to corona discharge, *IEEE Trans. Plasma Science,* 34, 1094-1098, Digital Object Identifier 10.1109/TPS.2006.876498 (2006).

20. B.-H. Youn, C.-S., Huh, Surface degradation of HTV silicone rubber and EPDM used for outdoor insulators under accelerated ultraviolet weathering condition, IEEE Trans. Dielectrics Electrical Insulation, 12, 1015-1024 (2005).

21. R. Atkinson, Kinetics of the gas-phase reactions of a series of organosilicon compounds with OH and NO_3 radicals and O_3 at 297$\pm$2 K, *Environ. Sci. Technol.*, 25, 863-866 (1991).

22. J. M. Jenkins, G. A. Olson, P. J. McFarland, D. O. Miller, W. H. Brune, Prodigious amounts of hydrogen oxides generated by corona discharges on tree leaves, *J. Geophys. Res., Atmos*., in revision

23. P. S. Nobel, Boundary layers of air adjacent to cylinders, *Plant Physiol.*, 54, 177-181 (1974).

24. F. Grum, L. F. Costa, Spectral emission of corona discharges, *Applied Optics*, 15, 76-79 (1976).

25. B. Ruscic, Active thermochemical tables: Sequential bond dissociation enthalpies of methane, ethane, and methanol and the related thermochemistry, *J. Phys. Chem A.*, 119, 7810-7837, https://doi.org/10.1021/acs.jpca.5b01346 (2015).

26. R. Ono, T. Oda, T., Measurement of hydroxyl radicals in pulsed corona discharge. *Journal of Electrostatics,* 55, 333-342. doi: 10.1016/S0304-3886(01)00215-7 (2002).